



Hybrid Mobile Robot Path Planning Using Safe JBS-A*B Algorithm and Improved DWA Based on Monocular Camera

Thai-Viet Dang¹ · Phan Xuan Tan²

Received: 20 January 2024 / Accepted: 24 September 2024 / Published online: 12 October 2024
© The Author(s) 2024

Abstract

This paper addresses the formidable challenge of enabling autonomous navigation in Mobile Robots (MRs), focusing on the development of advanced path planning strategies. Despite their pivotal role in diverse applications, they face challenges in dynamic settings due to limitation in existing Global Path Planning (GPP) and Local Path Planning (LPP) techniques. In response to this, we propose an innovative hybrid path planning approach that enhances the A* algorithm with a risk-aware heuristic function and integrates the Jump Point Search (JPS) technique for route optimization. Additionally, B-spline smoothing is employed for perceptually global trajectory refinement. Our approach also includes an innovative improvement to the Dynamic Window Approach (DWA) to align with the proposed enhanced A* algorithm for effective local navigation. Acknowledging the importance of high-quality input in path planning, we present substantial improvements to the IRDC-Net, a monocular-image semantic-segmentation model that we studied previously. Novel improvements include the integration of quantization and the Adam optimizer, along with the implementation of the Balanced Cross-Entropy loss function. These enhancements not only elevate the output quality of IRDC-Net but also reduce the model's training parameters. The experimental results demonstrate the performance and viability of the proposed algorithm. Ultimately, the hybrid MR's path planning algorithm exhibits proficiency across various tasks, particularly in addressing the challenge of evading moving obstacles to ensure the robot's safety while adhering to the global path.

Keywords A* algorithm · Dynamic window approach (DWA) · Monocular camera · Mobile robot · Path planning · Semantic segmentation

1 Introduction

Over the past few decades, mobile robots (MRs) have increasingly gained the attention of researchers from both academia and industry due to a rich set of applications in various areas like industry, agriculture, military, etc. MRs can replace humans in practical applications in harsh environments, such as performing firefighting and rescue missions [1]. Recently, the realm of MRs has witnessed a paradigm shift with the

advent of autonomous navigation, a feat largely dependent on the efficacy of path planning (PP). The essence of path planning lies in its ability to guide MRs through complex, dynamic environments, balancing the shortest route with the paramount need for safety. In this context, the development of robust path planning algorithms becomes a cornerstone for the advancement of MRs, necessitating continuous innovation to meet the evolving challenges of real-world applications [2–5].

Despite the leaps in technology, existing path planning methods still face considerable challenges. GPP techniques, pivotal for navigating in well-known, static environments, often struggle in dynamically changing settings. Typically, methods such as Dijkstra, A*, and D* have been the bedrock of GPP [4–7]. The Dijkstra algorithm, straightforward in static environments, tends to be less efficient and slower at optimizing paths in larger, more dynamic settings [6]. The A* algorithm, an evolution of Dijkstra, incorporates a heuristic function enabling faster identification of the shortest path on grid maps [7]. However, its planned trajectory might

✉ Thai-Viet Dang
viet.dangthai@hust.edu.vn

Phan Xuan Tan
tanpx@shibaura-it.ac.jp

¹ Department of Mechatronics, School of Mechanical Engineering, Hanoi University of Science and Technology, Hanoi 10000, Vietnam

² Shibaura Institute of Technology, Toyosu, Tokyo, Koto-Ku 135-8548, Japan

be too close to obstacles, potentially placing the MRs at risk of collision. The dynamic D*Lite algorithm, an advancement catering to dynamic environments, addresses issues of efficiency and energy consumption [8]. Despite its effectiveness in unknown environments, D*Lite suffers from certain limitations, such as slow planning efficiency, numerous path nodes and turning points in large-scale environments.

On the other side of the spectrum, LPP techniques are adept at real-time obstacle avoidance but lack the comprehensive oversight offered by GPP, often leading to suboptimal path decisions in the broader context of the robot's mission. To perform LPP, MRs often rely on methods like the Rapidly exploring Random Tree (RRT), the Artificial Potential Field (APF), and the DWA to navigate around obstacles [9]. The APF method is known for its high safety and smoothness levels in the operations in practical applications. However, its effectiveness is limited to local search areas, particularly when obstacles are near the target, potentially impeding the MRs' ability to reach their destination [10]. The DWA, as a technique to sample data from the constantly changing local environment, enables MRs to predict the next moving state based on their current state. Compared to APF, DWA achieves faster planning, ensures safety and reliability, and maintains robust real-time performance [10, 11]. However, while DWA effectively avoids both static and dynamic obstacles, its reliance on global environmental factors is a notable limitation.

Recognizing these gaps, in this paper, a novel hybrid approach to PP that synergizes the strengths of GPP and LPP is proposed. Particularly, we propose an enhanced A* algorithm, integrating a risk-aware heuristic function that dynamically adjusts to environmental changes, enabling safer and more efficient path planning. This novel approach is augmented by the application of the Jump Point Search (JPS) technique, which refines the path by eliminating redundant waypoints, thereby optimizing the route efficiency. Additionally, the B-spline transition method is integrated to smooth the global path ensuring the performance of tracking trajectory with the minimal change in steering angles. Complementing this, an innovative improvement to the DWA is introduced. This enhanced DWA is intricately designed to work in harmony with the global path insights provided by our enhanced A* algorithm. By doing so, it not only reacts to immediate obstacles but also aligns its maneuvering with the overall navigation strategy, ensuring a seamless integration of local and global PP considerations.

To provide better input for path planning, we present substantive enhancements to the IRDC-Net [12]. Typically, IRDC-Net is formed by a MobilenetV2 encoder and a lightweight Fully Convolutional Network (FCN) decoder with multi-scale fusion. To address imbalances in datasets, a replacement of the Binary Cross-Entropy loss function [4] with the Balanced Cross-Entropy loss function has been implemented [12]. This modification is

accompanied by a substantial reduction in the number of parameters utilized for model training. Based on captured images from monocular cameras, the proposed methodology adopts an IRDC-Net to extract features. This enables the accurate estimation of both the position and distance of obstacles within the robot's environment. Consequently, the acquired data contributes significantly to the resolution of complex challenges present in indoor environments in real-time, encompassing scenarios pertaining to both GPP and LPP. To enhance the efficiency and performance of IRDC-Net, quantization and the Adam optimizer are utilized.

The primary contributions of the paper are outlined as follows:

- Enhanced IRDC-NET: we propose an enhanced IRDC-NET, a lightweight semantic segmentation model based on a monocular camera, which improves perception quality. The integration of quantization and the Adam optimizer reduces computational time and model parameters while maintaining high accuracy in obstacle detection and environment understanding.
- Advanced GPP with Safe JBS-A*B algorithm: We enhance the A* algorithm with a risk-aware heuristic function and integrate the Jump Point Search (JPS) technique. This approach refines the global path by eliminating redundant waypoints and applying B-spline smoothing, resulting in a trajectory that closely aligns with the robot's kinematics, ensuring safer and more efficient PP.
- Enhanced LPP aligned with GPP: We introduce an improved DWA for LPP that synergizes with the global path insights provided by the enhanced A* algorithm. The integration allows DWA to not only react to immediate obstacles but also align its maneuvering with the overall navigation strategy, ensuring efficient navigation in complex environments with dynamic obstacles.
- We evaluate our proposal through experiments in simulated and real-world environments, demonstrating the practical navigational capabilities and effectiveness of the proposed hybrid path planning (HPP) algorithm.

The subsequent sections of the paper are structured as follows: Section 2 introduces the current state-of-the-art methods. The proposed architecture of lightweight IRDC-Net and network training are provided in Section 3. In Section 4, the hybrid MR's path planning is presented. Section 5 details both simulated and practical experiments. And Section 6 concludes the paper and future research developments.

2 Literature Review

In real-world scenarios, the MR's path-planning (PP) technology faces a growing challenge of managing progressively complex tasks. PP serves as a vital tactic in guiding a

robot through a perpetually shifting setting. Hence, numerous approaches merge the robust obstacle evasion capability of LPP algorithms with GPP to enhance efficiency [12, 13]. Consequently, the A* algorithm exhibits the redundant search nodes to increase both calculation scale and search time [14]. Zhao et al. fused JPS with the A* to diminish the number of extended nodes to less calculation time, boost search efficiency, and refine PP speed [15]. However, GPP encounters challenges with non-continuous curvature changes, insufficiently smooth turning points, in local search areas. Tang et al. employed HPP using third-degree B-spline to refine GPP but overlooked the obstacle region constraint, potentially causing paths to intersect obstacles in narrow spaces [16]. Song et al. introduced three path smoothers for optimizing GPP, yet computation time increases with the number of node count scales [17]. For ensuring safety in real-world, Zhang et al. factored in the distance of nodes from obstacles, incorporating threat value into heuristic evaluation [18]. Despite securing path safety, it is not suitable for large-scale intricate map environments in natural surroundings. When an MR encounters a complex environment, relying solely on a single GPP proves ineffective and inefficient in completing the multi-task, necessitating a fusion of global and local algorithms.

Tang et al. introduced HPP combining the A* with the APF to tackle PP in dynamic settings. However, the LPP performance was unsatisfactory in narrow areas with dynamic obstacles [19]. Wang et al. introduced a HPP blending an enhanced A* with the DWA to address the limitations of the path inflection points [20]. Then, the proposed HPP was added smoother algorithm in [21]. But they have yet overlooked temporary obstacle handling. Yasrab et al. suggested merging reinforcement learning with the A* to mitigate computational complexity during PP [22]. Next, Liu et al. developed this HPP with the novel best path selection [23]. Beed et al. integrated genetic algorithm with A* to shorten path length [24]. Tao et al. united the ant colony algorithm with A* to reduce expansion nodes and enhance search efficiency during path exploration [25]. Dang combined A* with the TEB to achieve smoother and safer planned paths [26]. Li et al. fused the enhanced D* Lite algorithm with sub-objective centered HPP, streamlining GPP and maintaining a secure distance [27].

In large-scale dynamic environments containing narrow gaps, the HPP achieves global optimization, dynamic obstacle avoidance, and smoothed paths. Lu et al. developed an HPP by utilizing the Global Voronoi diagram and D* [28]. Generated PP becomes smoother and more efficient. However, an existing drawback is its restriction to target points in the same direction. Imran et al. integrated the visual graph based GPP with the APF to gain both shortest path and obstacle avoidance safety [29]. Wu et al. proposed a HPP to combine the beetle antenna search with the APF to address

dynamic PP problems [30]. Its effectiveness and superiority require a large source of real-time data while moving in a large-scale dynamic environment. Kashyap et al. presented HPP using DWA to achieve the real-time optimal GPP. Although its DWA required the robot's dynamic characteristics for velocity space calculations [31]. Ma et al. proposed an improved HPP including such as follows: minimum snap trajectory generation, and timed elastic band for solving the PP's problem [32]. The HPP using DWA [33] provided the advanced driving assist systems to control vehicle velocities and automatically assist obstacle avoidance. Moreover, the driving assist system based on HPP with image based DWA [34] successfully utilized the human vehicle cooperative navigation system. Therefore, in complex environments, the real-time HPP combining with DWA has enhanced MR's efficiency and flexibility.

In summary, current research on hybrid path planning (HPP) has made significant strides in combining global path planning (GPP) and local path planning (LPP) techniques to enhance robot navigation in complex environments. However, many of these methods face specific limitations such as suboptimal handling of dynamic obstacles, and challenges in achieving smooth trajectory planning.

3 IRDC-Net

The backbone network and the whole architecture of IRDC-Net comprise most of the lightweight semantic segmentation systems. Next, two key modules of inverted residual (IR) and despise convolution (DC) in IRDC-Net are detailed. Finally, the authors present additional information of model training and quantization techniques to obtain the lightweight network version in comparison with previous network architecture [4].

3.1 Network Architecture

An FCN-based network capable of achieving instantaneous pixel-wise labelling with respectable segmentation performance [35, 36]. Yang et al. [37] utilized to improve a low-resolution, approximate output prediction by integrating with previous layers. Model's output provides reasoning on both a local and global scale [4, 12, 37]. As illustrated in Fig. 1, the proposed model is founded upon the MobilenetV2 backbone [38]. The input to the model consists of 224×224 images, and image features are extracted using 15 inverted residual (IR) blocks, in Fig. 1a. By augmenting several convolutional layers in the intermediate layers [39], the feature extraction procedure is enhanced in comparison to the conventional residual mechanism [35]. To decrease the quantity of model parameters, the IR blocks are additionally linked to DC classes, in Fig. 1b.

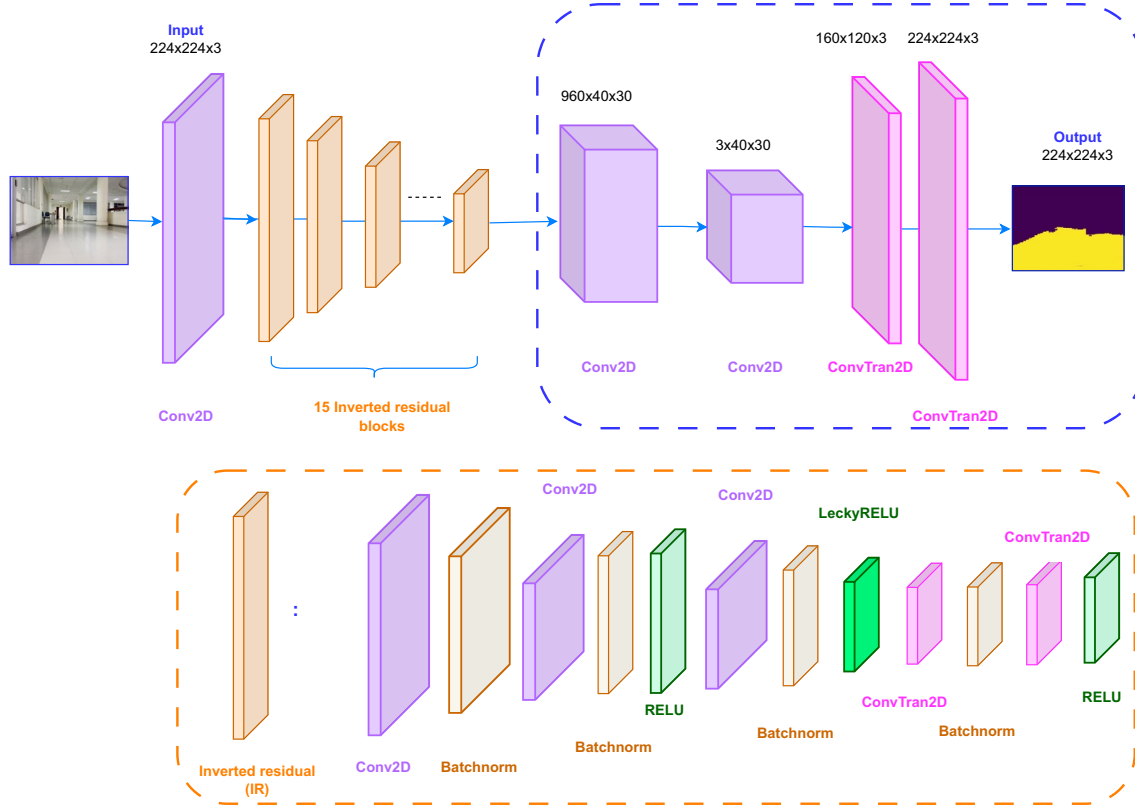


Fig. 1 Proposed lightweight semantic segmentation IRDC-Net containing the architecture of two main clusters such as (a): DC and (b): IR [12]

In the initial layer, a 1×1 convolution is implemented using the Relu6 activation function. To reduce the dimensions of the subsequent 3×3 depthwise convolution, the second layer is indistinguishable. The third layer subsequently consists of a 1×1 convolution without activation function. "Relu" Block is utilized instead of "Linear" Block. Two residual blocks: "stride = 1" and "stride = 2" are utilized to supply intermediate layers, in Fig. 2a and b, respectively. The distinction between IR and the initial representation resides in the modification implemented for the skip connection in MobilenetV2. Skip connection helps both preserve information in the first layers (low-level features) and learn semantic information in deeper layers (high level features). Besides, the phenomenon of vanishing gradients is avoided because of deciding the path of information when the gradient propagates back to the first layers. Moreover, skip connection structure combined with "Relu" block, the problem of vanishing gradient is completely solved. I/O channels are reduced by the architecture of bottleneck layer [38], at each residual block, from Fig. 2c to f. When the skip connections are conducted, IR links the layers. On the contrary, the intermediate layers reduce the input and output channels of the original residuals utilized in ResNet [40]. Then, on the entire input channel, DC replaces a single kernel (filter) to conduct convolutional computations to reduce the training

parameters and computation scale. The convolution computation is applied on all channels, this conventional convolution layer can be employed to merge features obtained from distinct channels.

3.2 Model Training

The proposed model was trained on four datasets: Cityscapes, Duckie-dataset, KITTI, and TaQuangBuu's (TQB) dataset [12]. The investigations are conducted utilizing the subsequent configuration: Intel® Core™ i7-11800H Processor, RAM 32 GB, Nvidia 2080TI 12 GB VRAM, Python 3.11.0, TensorFlow 1.4, and 64-bit operating system. Based on real-world information collected from the TQB image updating self-collected images [4, 12, 39], a significant proportion of pixels designated as obstacles have been determined to be located along the path. The Binary Cross Entropy loss function was used in our previous investigations [4, 39] to distinguish between two classes, namely available and unavailable regions. This resulted in an imbalance, however, in the data. When employing Binary Cross Entropy as the loss function, the learning model exhibits a tendency to prioritize the more frequently occurring object within the dataset. One potential solution to the issue could be to augment the training data with additional instances of

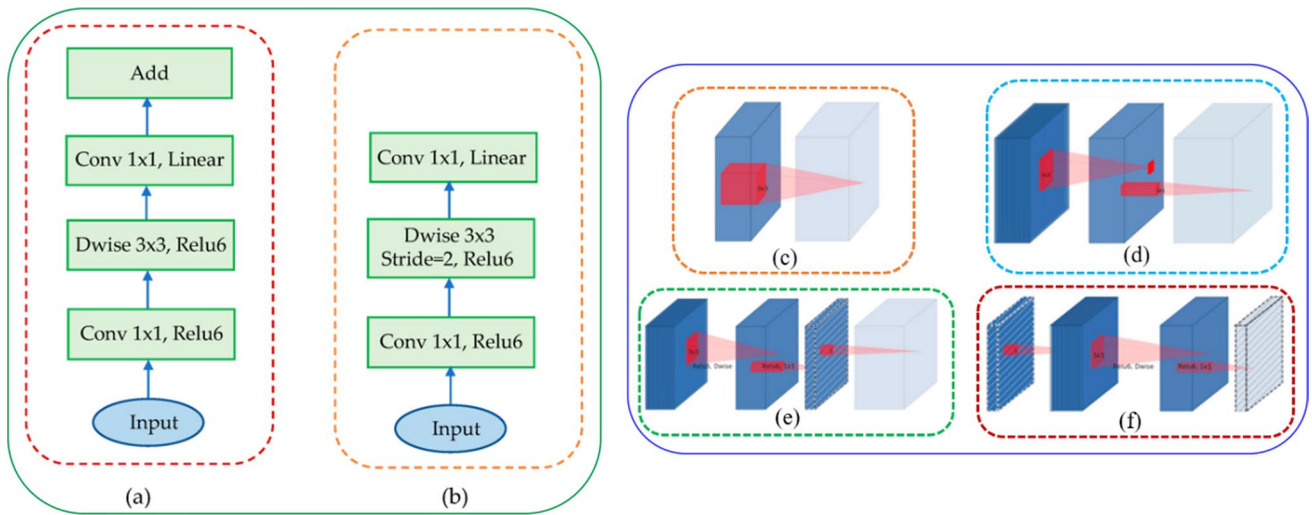


Fig. 2 MobilenetV2 with two residual blocks of (a) strike = 1 and (b) strike = 2 [12]; convolutional blocks of (c) regular, (d) separable, (e) linear bottleneck, and (f) bottleneck [38]

the less dominant class. Consequently, we suggest implementing the revised Balanced Cross-Entropy (BCE) loss [12] in following Eq. (1):

$$L_{Balanced-CE}(y, \hat{y}) = \{\beta \times y \log(\hat{y}) + (1 - \beta) \times (1 - y) \log(1 - \hat{y})\} \quad (1)$$

where \hat{y} : the class SoftMax probability and y : the ground truth associated with the prediction. $\beta = 1 - \frac{y}{H \times W}$ and $H \times W$ provides the pixel count of the entire image. Moreover, β is employed to modify the quantity of false positives and false negatives in the following ways: $\beta > 1$ decreases the quantity of false negatives or $\beta < 1$ reduces the quantity of false positives.

In addition, the BCE function is applicable to segmentation issues involving multilayer images. The BCE function exhibits optimal performance when applied to a wide range of datasets, but especially when asymmetrical. As a result, path planning will operate with enhanced efficiency across diverse internal contexts. To optimize the BCE, the Adam optimizer [41] was implemented. Training the IRDC-Net lasted 100 epochs at a learning rate of 0.001. To improve the quality of the unprocessed input, the data set underwent pre-processing using Gaussian blur [42] and Gaussian noise [43] prior to undergoing the IRDC-Net.

Although the image quality will be compromised when the algorithms are implemented, they can generate more generalized datasets that improve the quality of the segmentation model. By employing the quantization technique [44], the dimensions and computational demands of a ML model are diminished through the representation with diminished precision. In the training portion of a machine-learning model, parameters such as the weight and bias are often represented with high precision utilizing

floating-point data. However, the substantial storage and computational resources required for this may pose a challenge when attempting to deploy the model on devices that have limited resources, such as embedded microcontrollers or mobile devices. Through the implementation of quantization, wherein the model's parameters are represented as limited-precision integers or real-number data, it is possible to simultaneously enhance computational performance and decrease storage requirements. By employing quantization techniques including weight quantization, activation quantization, or a hybrid approach involving both, this objective can be accomplished. To reduce the dimensions of the model, FP32 (32-bit floating-point precision) downsizes to FP16 (16-bit floating-point precision), in Fig. 3.

4 Hybrid Path Planning Based on Ground Plane Segmentation

4.1 Ground Plane Segmentation

Firstly, the image coordinates will be transformed into the image plane according to the focal length of the camera. Then, the second transformation displays the intrinsic camera matrix to convert the image plane to the pixel plane. The compress effect becomes more pronounced as the object's distance increases because the focal length remains constant, the ratio between coordinates gets smaller. In addition, the authors fix the perspective distortion in Fig. 4 by utilizing homography transformation to set up the pixel plane for MR path planning. To illustrate the connection between the image plane ($p: 3 \times 1$) and world coordination ($W: 4 \times 1$), the transformation described by Eq. (2):

Fig. 3 The quantization in proposed network

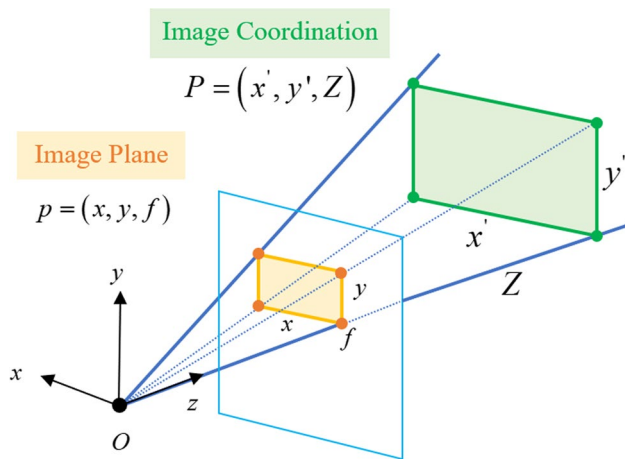
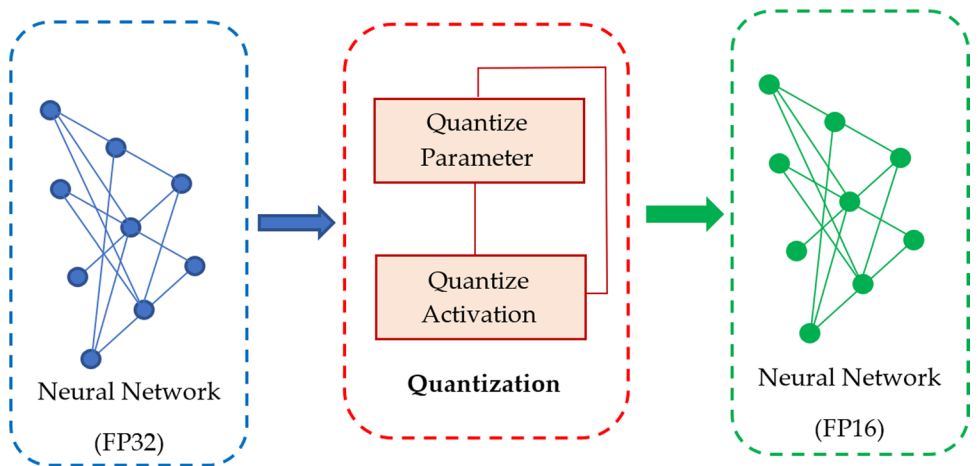


Fig. 4 A perspective projection

$$p = M_{\text{int}} \times M_{\text{ext}} \times W \quad (2)$$

where M_{int} : 3×4 intrinsic parameters, and M_{ext} : 4×4 extrinsic parameters. Because the camera poses are fixed to form MR's bird's eye view.

In the ground surface ($Z=0$), the homography matrix $H : 3 \times 3$ represents the transformation between four points (x, y) of the perspective plan 1 and four points (x', y') of the perspective plan 2 based on bird's eye view [45], in following Eq. (3).

$$H = \begin{bmatrix} h_{11} & h_{12} & h_{13} \\ h_{21} & h_{22} & h_{23} \\ h_{31} & h_{32} & h_{33} \end{bmatrix}; x = \frac{h_{11}x' + h_{12}y' + h_{13}}{h_{31}x' + h_{32}y' + h_{33} + 1}; y = \frac{h_{21}x' + h_{22}y' + h_{23}}{h_{31}x' + h_{32}y' + h_{33} + 1} \quad (3)$$

The system of eight equations involving eight parameters (see Eq. (4)) can be solved using four points whose coordinates are known in Eq. (3):

$$\begin{bmatrix} \text{Point 1} \\ \text{Point 2} \\ \text{Point 3} \\ \text{Point 4} \end{bmatrix} = \begin{bmatrix} x_1 & y_1 & 1 & 0 & 0 & 0 & -x_1x'_1 & -y_1x'_1 \\ 0 & 0 & 0 & x_1 & y_1 & 1 & -x_1y'_1 & -y_1y'_1 \\ x_2 & y_2 & 1 & 0 & 0 & 0 & -x_2x'_2 & -y_2x'_2 \\ 0 & 0 & 0 & x_2 & y_2 & 1 & -x_2y'_2 & -y_2y'_2 \\ x_3 & y_3 & 1 & 0 & 0 & 0 & -x_3x'_3 & -y_3x'_3 \\ 0 & 0 & 0 & x_3 & y_3 & 1 & -x_3y'_3 & -y_3y'_3 \\ x_4 & y_4 & 1 & 0 & 0 & 0 & -x_4x'_4 & -y_4x'_4 \\ 0 & 0 & 0 & x_4 & y_4 & 1 & -x_4y'_4 & -y_4y'_4 \end{bmatrix} \begin{bmatrix} h_{11} \\ h_{12} \\ h_{13} \\ h_{21} \\ h_{22} \\ h_{23} \\ h_{31} \\ h_{32} \end{bmatrix} = \begin{bmatrix} x'_1 \\ y'_1 \\ x'_2 \\ y'_2 \\ x'_3 \\ y'_3 \\ x'_4 \\ y'_4 \end{bmatrix}, \quad (4)$$

where Point 1 = $\begin{bmatrix} x'_1 \\ y'_1 \end{bmatrix}$, Point 2 = $\begin{bmatrix} x'_2 \\ y'_2 \end{bmatrix}$, Point 3 = $\begin{bmatrix} x'_3 \\ y'_3 \end{bmatrix}$, and Point 4 = $\begin{bmatrix} x'_4 \\ y'_4 \end{bmatrix}$. Therefore, based on Eq. (4), the homography transformation [45] is applicable to any set of four points on that plane, in Fig. 5.

Finally, MR's perception is constructed based on the pixel plane in the bird's eye view, in Fig. 6.

4.2 Global Path Planning Based on JBS-A*B Algorithm

Following this, the ground plan image will be subdivided into grid cells. The current coordinates are displayed in the lower-center position of the image, in Fig. 7.

Based on the cell division in Fig. 7, the known environment is represented by the grid-map in Fig. 8, where obstacles are represented by black cells and conversely, white cells permit to move.

The A* algorithm designs the HF to select the closest nodes to the target [7]. Hence, the search process rapidly determines the shortest possible route from S to G, in Fig. 8a. The traditional A*'s HF is shown in Eq. (5):

$$f(n) = g(n) + h(n), \quad (5)$$

where n: the current node, $f(n)$: the total cost evaluation, $h(n)$: the predicted cost from n to G, $g(n)$: the actual cost from

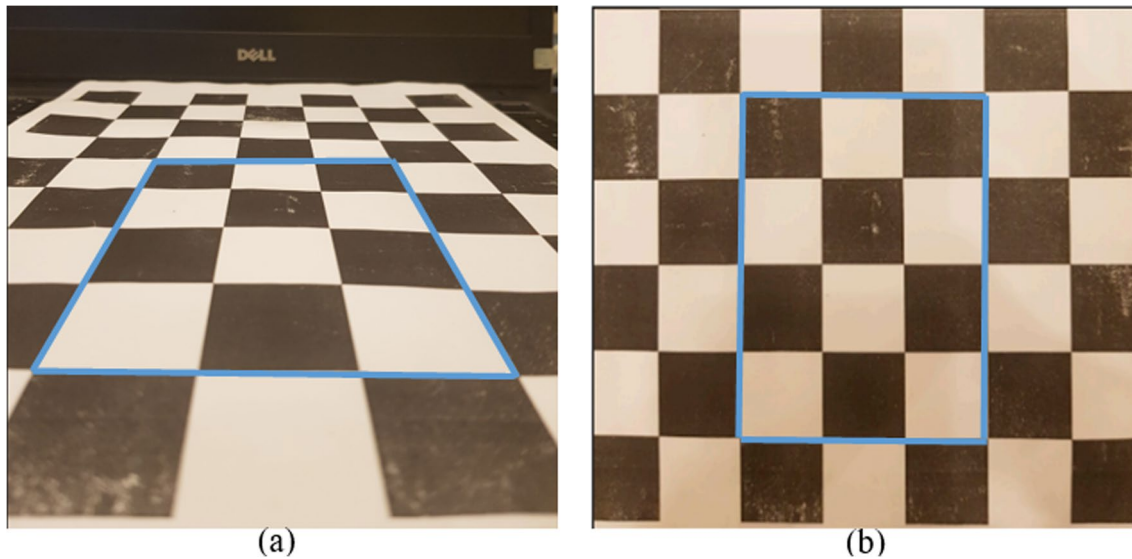


Fig. 5 The homography transformation from (a) image plane to (b) pixel plane in bird's eye view using a checkerboard

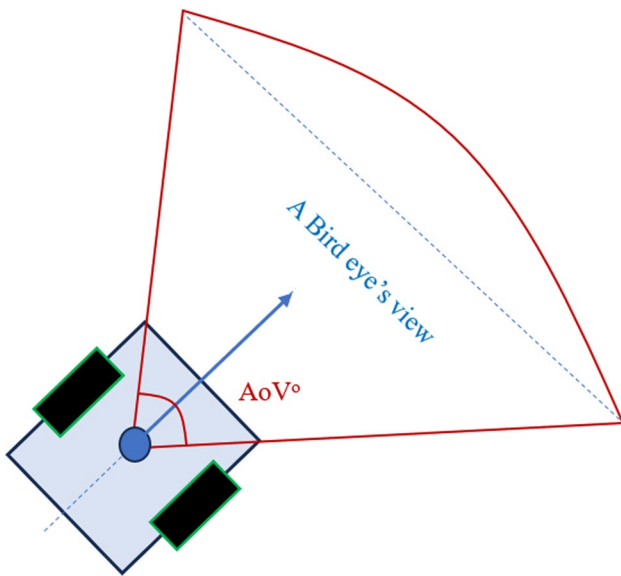


Fig. 6 The bird eye's view of the MR

n to the following node. However, the shortage of information about the size and kinematic leads to the MR's path easily colliding with the edges of obstacles. To fix the above problem, a redesigned environment model will include additional risk zones around obstacles, in Fig. 8b. Depending on the danger level of collision, the distance of the danger zone to the obstacle is determined according to the change of grey zone. Based on new grid-map, A* algorithm utilizes a new HF in Eq. (6):

$$f(n) = g(n) + h(n) + r(n), \quad (6)$$

where $r(n)$: the risk cost depending on the distance to obstacle at each risk level. Safe coefficient plays an important role of obstacle avoidance path planning in dynamic environments. The simple environment has less obstacle, $f(n)$ will be near to the actual distance. But, in complex environments, the actual distance will be larger than value of $f(n)$. When the distance from n to G exceeds the value of $h(n)$, the search area is expanded. Hence, the number of search nodes is increased, and the overall efficiency is simultaneously reduced. On the contrary, the number of search nodes is decreased and search computational process becomes faster. Therefore, the current MR's position in the grid-map causes to revise $h(n)$, in Eq. (7):

$$f(n) = g(n) + \left(d + \frac{1}{D} \right) h(n) + r(n), \quad (7)$$

where d and D : the distance from n to G, and to S, respectively. In A* search algorithm, $h(n)$, is calculated by Manhattan distance $h_M(n)$ in Eq. (8):

$$h_M(n) = |x_G - x_C| + |y_G - y_C|, \quad (8)$$

and Euclidean distance $h_E(n)$ in Eq. (9), separately.

$$h_E(n) = \sqrt{(x_G - x_C)^2 + (y_G - y_C)^2}, \quad (9)$$

where (x_G, y_G) : G's coordinated and (x_C, y_C) : C's coordinate, respectively.

If A* algorithm uses Eq. (6), the Manhattan symmetric path is constructed by 4-neighborhoods search technique in Fig. 9a. Otherwise, the Euclidean symmetric path is based on 8-neighborhoods search technique in Fig. 9b.

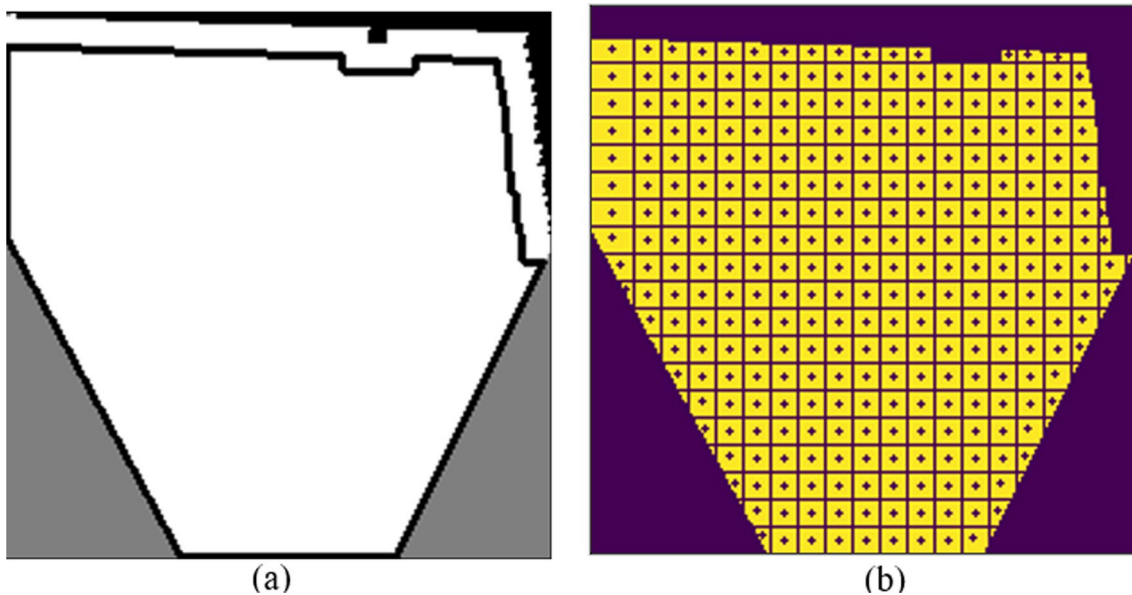


Fig. 7 The moveable region with (a) the pixel plane and (b) the grid cell

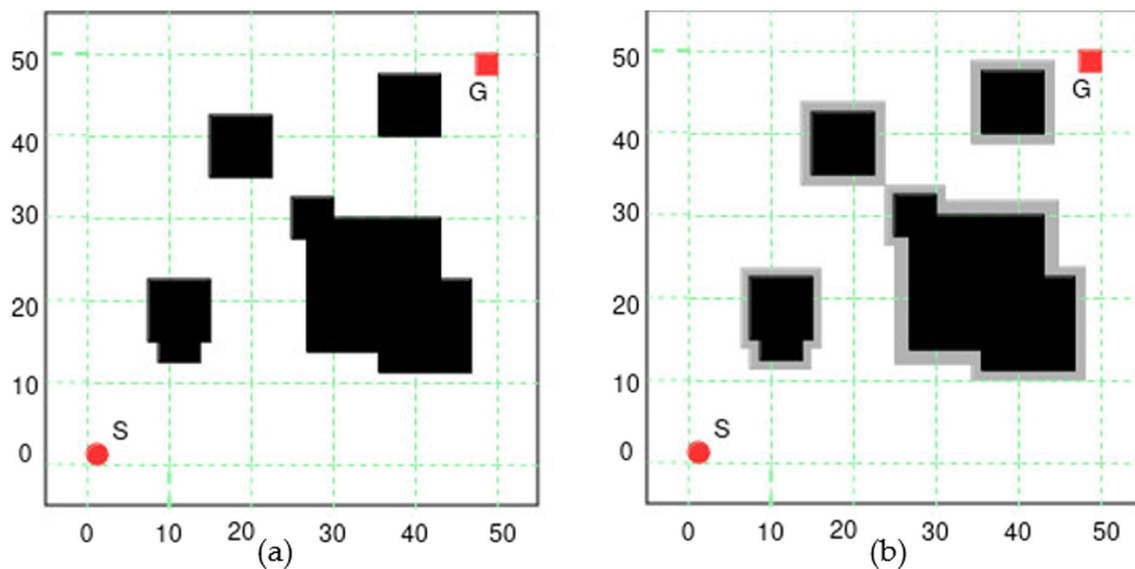


Fig. 8 MR's environment based on grid method with (a): without risk regions and (b): having risk regions

The proposed global safe A* path planning is designed by the Euclidean symmetric path to ensure the optimal path connecting from S to G. In addition, the enhanced A* path planning will restrict the extension of search nodes into risk regions. The revised $h(n)$ in Eq. (7) improves search effectiveness. Therefore, the proposed global safe A* algorithm guarantees that the initially planned paths maintain a secure distance from obstacles.

Based on the enhanced A* algorithm, Jump Point Search (JPS) is utilized to solve the aforementioned problems in

a large-scale map environment, including many extended nodes, high computational scale, and low search efficiency. In complex local regions, JPS creates more path nodes to avoid obstacles. Hence, subsequent trajectory optimization and smooth trajectory have been more difficult. To remedy this situation, the turning point is eliminated to improve the efficiency of the search algorithm and to support MR's trajectory smoothness, in Fig. 10. JPS's description includes the following steps. Traditional A* algorithm search results are a series of path points P_k . In Fig. 10a, if there exists a

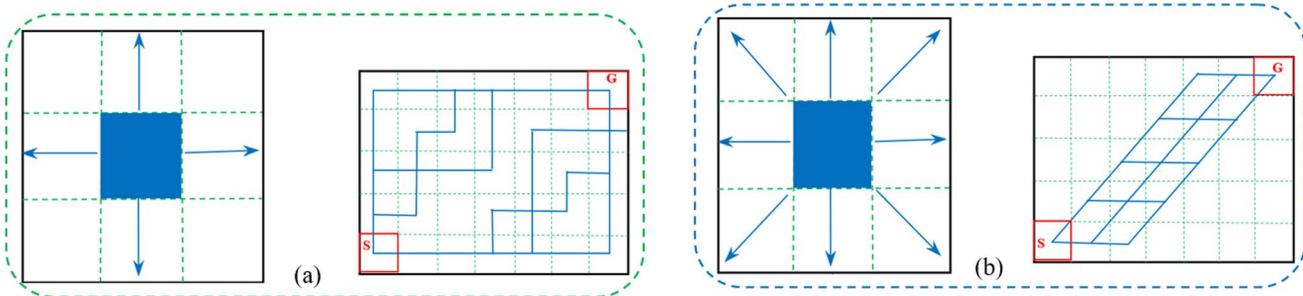


Fig. 9 The symmetric path planning is based on A* algorithm with (a) 4-neighbors directions and the Manhattan symmetric path and (b) 8-neighbors directions and the Euclidean symmetric path

set of three points (P_1, P_2, P_3) of P_k , the red dashed line P_1P_3 satisfying without touching obstacles will be replaced with the continuous black polyline $P_1P_2P_3$. The distance P_1P_3 is significantly shorter than and a redundant path point P_2 has been eliminated. The procedure will be repeated until the path reaches the desired location G.

In Fig. 10b, from the obtained global path, JPS is used for creating the path $P_1P_2P_3P_4P_5$ from S to G. Then, JPS is re-applied to remove the redundant points of P_1, P_3, P_4 , and P_5 . Thus, the objective of enhanced red path planning SP_2G would be entirely attained. JPS can locate the shortest path more quickly than the A* algorithm because it avoids analyzing numerous grid nodes that are not on the shortest path. Lastly, the safe JPS-A* algorithm ensures the search algorithm's efficiency and speed are substantially enhanced.

The path planning method can find an optimal path without considering the MR's kinematic model. So, the path is not smooth. Its curved segments usually are not continuous.

MR's smoothed path refers to the absence of abrupt changes in direction or speed while tracking trajectory. A MR's navigation will be aided by a JBS-A*B algorithm using B-spline curves depicted by Eq. (10).

$$B(t) = \sum_{i=0}^4 N_{i3}(u)P_{ti}, \quad (10)$$

where P_{ti} are the control path nodes and $N_{i3}(u)$ are the B-spline basis functions of the third degree. As an example, in Fig. 11a, with the set of three points P_{i-1}, P_i , and P_{i+1} , the B-spline will require five control path nodes of $P_{t0}, P_{t1}, P_{t2}, P_{t3}$, and P_{t4} to satisfy with Eq. (9). Besides, P_i must coincide with P_2 . Furthermore, P_{i-1}, P_{t0}, P_{t1} , and $P_i(P_{t2})$ are collinear. Simultaneously, P_{i+1}, P_{t4}, P_{t3} , and $P_i(P_{t2})$ are collinear. Hence, the B-spline curve will be created to smooth the polyline $P_1P_2P_3$. Furthermore, the third-degree B-spline curve is

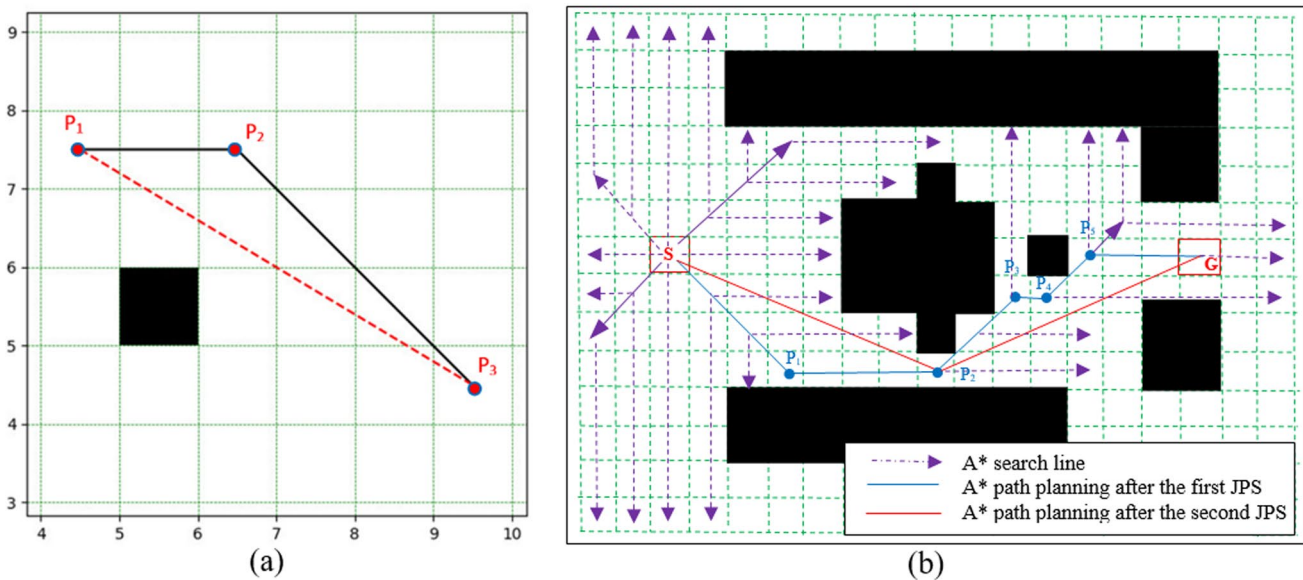


Fig. 10 JPS algorithm with (a) a set of three path points and (b) enhanced A* algorithm with JPS

applied to the safe JPS-A* algorithm to optimize the MR's trajectory based on the global A* path planning, in Fig. 11b. Consequently, ensuring a smoothed tracking trajectory is a crucial element to improve the efficiency, reliability, and safety of the MRs.

4.3 Real-Time Local Path Planning Based on DWA

Based on the known grid-map, GPP based on JBS-A*B algorithm ensures the MR's ability to respond to multi-tasks such as feasible connecting from S to G with the shortest distance, avoiding obstacles and smoothing the trajectory. However, GPP cannot handle dynamic obstacles changing their position [7, 39]. Therefore, LPP based on real-time sensor data [10] deals with dynamic obstacles. DWA [10, 11] guarantees the local path of the MR's velocity over an interval of time with the global planning guidance. The MR precisely replicates its trajectory and avoids any obstacles, in Fig. 12.

During the time interval Δt , the kinematics model of MR is expressed in following Eq. (11):

$$\begin{cases} x(t+1) = x(t) + v\Delta t \cos \theta \\ y(t+1) = y(t) + v\Delta t \sin \theta \\ \theta(t+1) = \theta(t) + \omega \Delta t \end{cases} \quad (11)$$

where x, y : the MR's coordinate positions in the environment; v : the MR's velocity; ω : the MR's angular velocity; θ : the MR's heading angle.

Within the velocity search space, the sampled velocities are limited by a certain range of many groups (v, ω) derived by the MR's movement in the real-time environment. All required

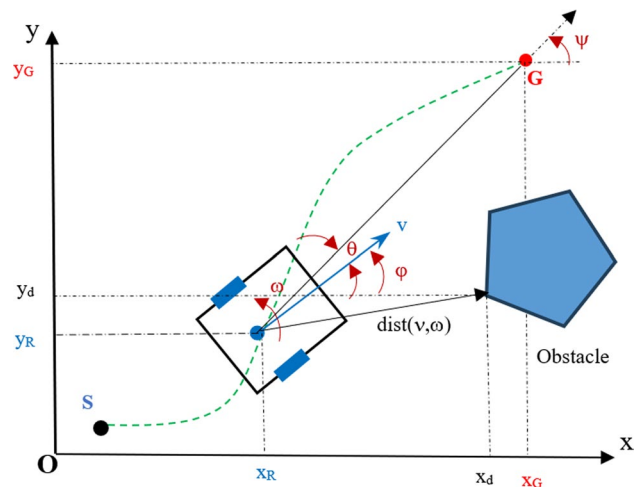


Fig. 12 MR's model of tracking global path planning

constraints including the MR's velocity, the MR's acceleration, and the minimal distance to obstacles are described in Equations from (12) to (14), respectively. At first, the MR's velocity constraint v_s is illustrated as:

$$v_s = \left\{ (v, \omega) \mid v \in [v_{\min}, v_{\max}] \cap \omega \in [\omega_{\min}, \omega_{\max}] \right\}, \quad (12)$$

where v_{\min}, v_{\max} : the maximum and minimum velocity, respectively and $\omega_{\min}, \omega_{\max}$: the maximum and minimum of angular velocity, respectively. Next, the actual velocity v_a in Eq. (13) is constrained due to the influence of motor torque, and it is closely linked to the angular acceleration ω of the MR.

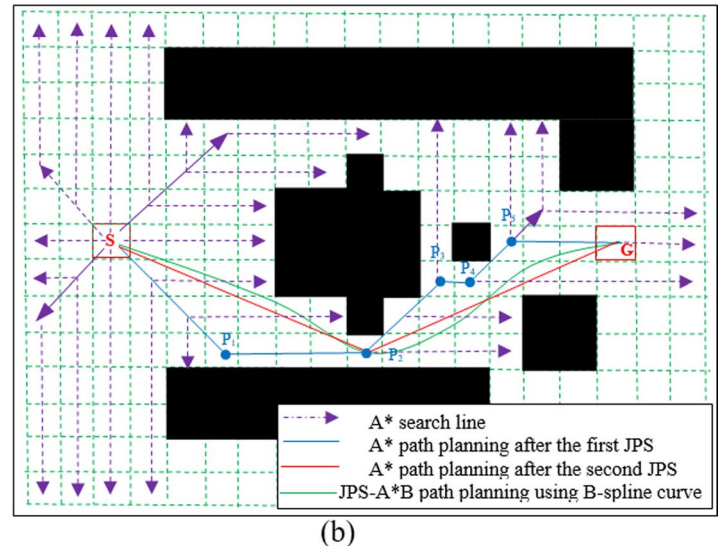
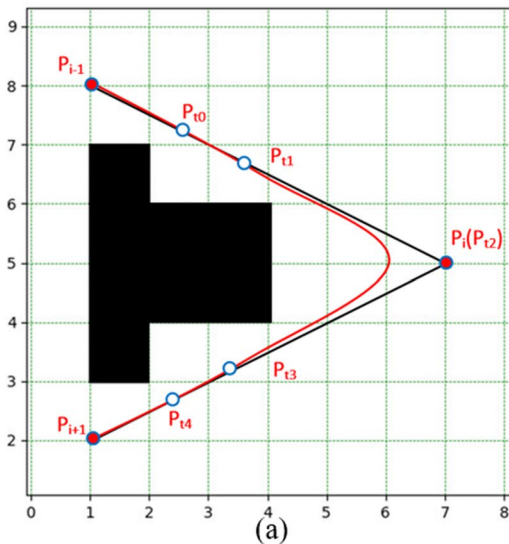


Fig. 11 The third-degree B-spline curve with (a) a set of three path points (P_{i-1}, P_i, P_{i+1}) and (b) the safe JPS-A*B path planning using the third-degree B-spline curve

$$v_a = \left\{ v, \omega \mid v \in [v_c - v_l \Delta t, v_c + v_u \Delta t] \cap \omega \in [\omega_c - \omega_l \Delta t, \omega_c + \omega_u \Delta t] \right\}, \quad (13)$$

where v_c and ω_c : the current velocity and angular velocity, respectively; v_u and v_l : maximum acceleration and deceleration of the velocity, respectively; ω_u and ω_l : maximum acceleration and deceleration of the angular velocity, respectively. Finally, in local regions, the MR maintains a fixed distance from obstacles. When discovering the moving obstacles in the DWA's area, the MR must stop at the moment just before collision. Obstacle distance constraint is represented by the maximum deceleration condition in Eq. (14). The MR's velocity v_d must satisfy the following conditions.

$$F(v, \omega) = \sigma \{ \alpha * head(v, \omega) + \beta * s_dist(v, \omega) + \delta * d_dist(v, \omega) + \gamma * vel(v, \omega) \}, \quad (15)$$

where $head(v, \omega)$: the azimuthal deviation effectively ensuring the MR follows the locally optimal path while maintaining the robot's movement direction to reach the global path's target point; $s_dist(v, \omega)$ and $d_dist(v, \omega)$: the distance between the MR's predicted path end with the nearest static obstacle and the nearest dynamic obstacle, respectively; $vel(v, \omega)$: the velocity of the current simulated trajectory; σ : the filtering coefficient, and α, β, δ , and γ : the weighting coefficient. Hence, the trajectory containing the minimum value of $F(v, \omega)$ is designated as the optimal trajectory. The dynamic window approach's objective function is depicted in Eq. (15) along with the primary distances and angles needed. Synthetic in the synthetic search velocity space v_r in the Fig. 13.

Based on the moving along the global path of the robot in Fig. 12 and DWA representation in Fig. 13 and, the target heading angle θ is determined by Eq. (16).

$$\theta = \psi - \varphi = \tan^{-1} \frac{y_G}{x_G}, \quad (16)$$

$$head^*(i) = \frac{head(i)}{\sum_{i=1}^n head(i)}; s_dist^*(i) = \frac{s_dist(i)}{\sum_{i=1}^n s_dist(i)}; d_dist^*(i) = \frac{d_dist(i)}{\sum_{i=1}^n d_dist(i)}; \text{ and } vel^*(i) = \frac{vel(i)}{\sum_{i=1}^n vel(i)}. \quad (19)$$

where i: the current evaluated trajectory points and n: the sampled trajectory points. Through iteratively modifying the weight coefficient and optimizing the objective function $F(v, \omega)$, the MR is capable of simultaneously traversing the designated path while evading obstacles at the most rapid velocity possible given the constraints. Equations from (15) to (19) indicate the DWA evaluation function $F(v, \omega)$ is efficacious. Dynamic obstacle avoidance performance makes it exceedingly challenging to devise a globally optimal path

$$v_d = \left\{ (v, \omega) \mid v \leq (2dist(v, \omega) \cdot v_l)^{1/2} \cap \omega \leq (2dist(v, \omega) \cdot \omega_l)^{1/2} \right\}, \quad (14)$$

where $2dist(v, \omega)$: the shortest distance from the obstacle to the MR's local path corresponding to (v, ω) .

Although, all constraints in Equations from (12) to (14) are satisfied, the DWA's evaluation function must be optimized to successfully find the JPS-A*B global optimal path. An azimuth evaluation $head(v, \omega)$ is added to the evaluation function while guaranteeing multi-tasks such as shortest path, dynamic obstacle avoidance and smoothness. The DWA's evaluation function of MR is expressed in Eq. (15):

$$F(v, \omega) = \sigma \{ \alpha * head(v, \omega) + \beta * s_dist(v, \omega) + \delta * d_dist(v, \omega) + \gamma * vel(v, \omega) \}, \quad (15)$$

where θ : target heading angle; ψ : target heading angle with global frame; and φ : MR heading angle with global frame. Hence, Eq. (16) yields to $head(v, \omega)$ illustrated in Eq. (17) as follows:

$$head(v, \omega) = 180^\circ - \theta. \quad (17)$$

Next, $dist(v, \omega)$ is computed in Eq. (18): the distance between the robot's center (x_R, y_R) and the nearest obstacle (x_d, y_d) in Fig. 12. Notably, obstacles are classified as either static or dynamic and. Then, the distances to them are $s_dist(v, \omega)$ and $d_dist(v, \omega)$, respectively.

$$dist(v, \omega) = \sqrt{(x_d - x_R)^2 + (y_d - y_R)^2}. \quad (18)$$

Finally, $vel(v, \omega)$ is calculated as the robot's linear velocity along the axis v, as illustrated in the Fig. 16. Based on Eq. (15), to satisfy the prerequisites for MR's smoothed trajectory, $head(v, \omega)$, $s_dist(v, \omega)$, $d_dist(v, \omega)$, and $vel(v, \omega)$ are normalized in the following Eq. (19).

based on spiritual information about the global environment, as its fatal flaw is that it falls into the local area and is unable to reach its destination. Information from the GPP will be incorporated into the evaluation function using the JBS-A*B algorithm. Therefore, in Eq. (20), which measures the azimuth deviation between the end of the simulated trajectory and the leap point closest to the current trajectory, $head(v, \omega)$ is substituted for $JPS_head(v, \omega)$ in Eq. (15).

$$F(v, \omega) = \sigma \{ \alpha * JPS_head(v, \omega) + \beta * s_dist(v, \omega) + \delta * d_dist(v, \omega) + \gamma * vel(v, \omega) \}. \quad (20)$$

In dynamic path planning, the improved DWA guarantees a seamless local optimal path that follows the contour of the optimal GPP path, in Fig. 14.

5 Experimental Results and Discussion

The MR's path planning based on the safe JBS-A*B algorithm and improved DWA (20) is constructed according to the optimal navigation strategy, in Fig. 14.

Firstly, over one thousand two hundred images were self-collected by the author from the TQB library [12]. The dimensions of the image input were 960 by 1280 pixels. The ultimate assessment of IRDC-Net's performance was conducted on a backdrop image depicted in Fig. 15, which comprised a multitude of obstacles and intersections.

Figure 16 shows the Accuracy, Loss, and mIoU in the training and validation process when input images were taken from the TQB data set. The training model quality parameters obtained ensure the successful response of the IRDC-Net.

In Table 1, on the same TQB data set, the quality of the IRDC-Net is much better than the FCV-VGG-16 [4]. Furthermore, to serve computational capabilities, and minimize processing time and system resources, IRDC-Net also reduced the number of segmentation model training parameters from 25 million parameters to 3.3 million parameters. The above results demonstrate the feasibility and advantages of IRDC-Net compared to FCN-VGG 16 when producing the ground plane segmentation used as input data for MR's path planning. The proposed segmentation model's specifications from TQB data set are described in Table 2.

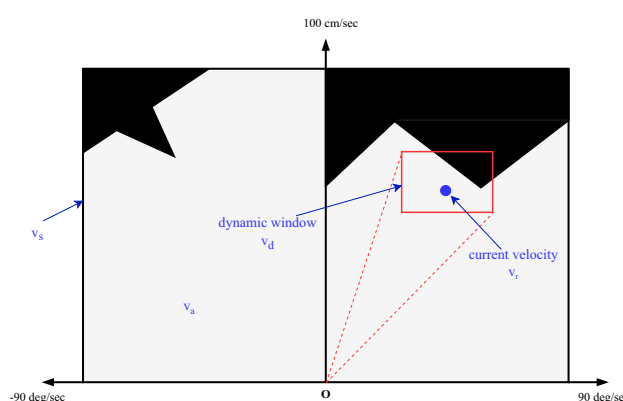


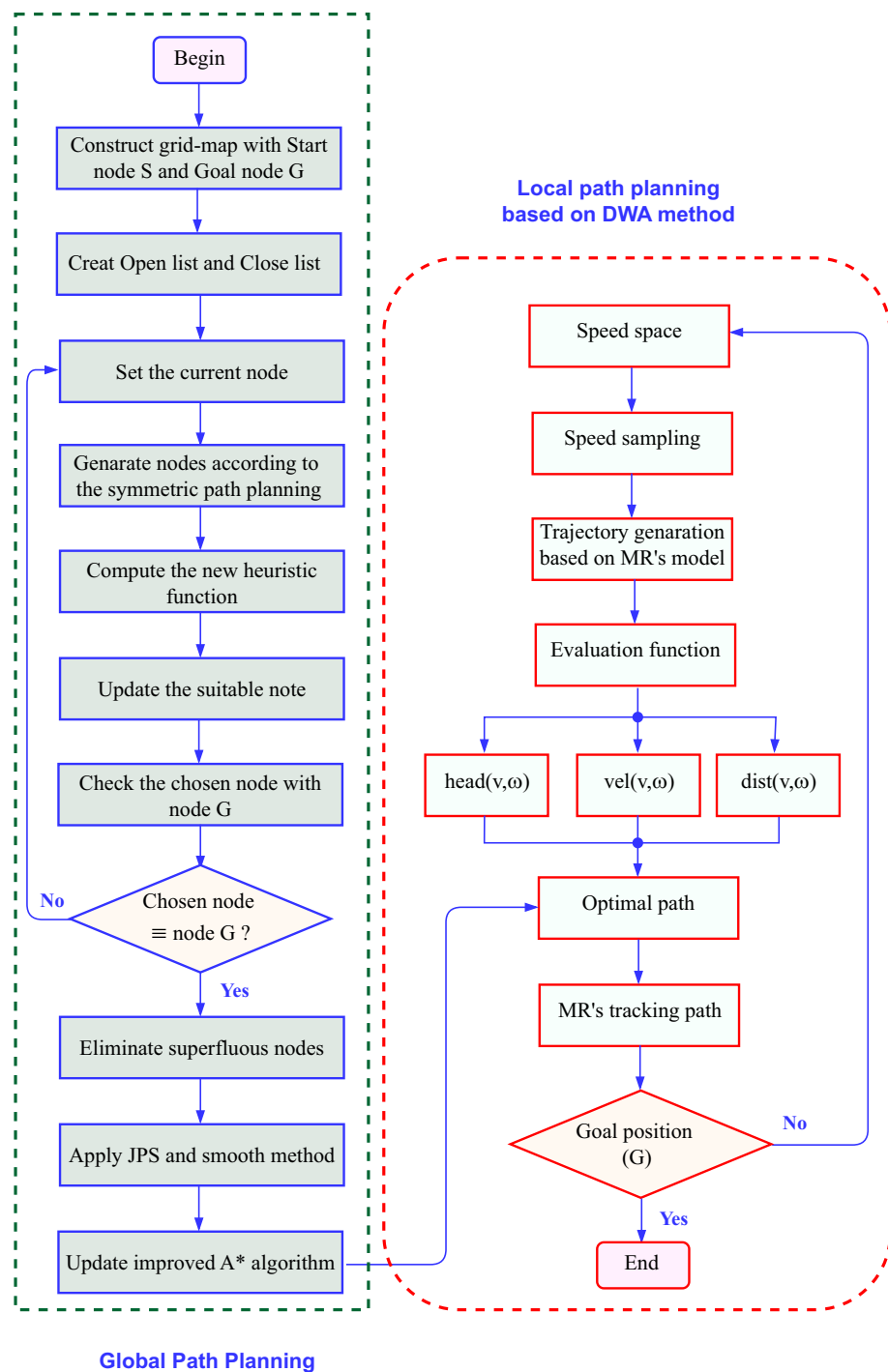
Fig. 13 The relationship between MR's velocity constraints: v_s , v_a , v_d and v_r in DWA

Based on the ground plane segmentation and MR's perception in the bird's eye view, the author intends to generate a moving path utilizing the frontal plane as input and employs the GPP based on A* algorithm, in Fig. 17. To begin, a safe area devoid of collisions is generated by applying heat to the unoccupied region. The ground plan image will subsequently be partitioned into grid cells. The present location is identified at the image's bottom center. Scenario 1 has a simple obstacle in the grid map. Obstacles are selected at different levels of danger based on the distance of the safety zone surrounding the obstacle, in Fig. 17a. The author utilizes the centroid of each cell to compute for the GPP, in Fig. 17b.

A comparison of the performance of the A* path and the path produced by integrating the risk cost. Then, results continue to analyze and reinforce the important role of JPS and B curves in the GPP based on JBS-A*B algorithm, in Fig. 18. In Fig. 18a, A* path planning will collide with the edge of the obstacle due to the lack of risk factor (red dot line). Additionally, a safe coefficient is incorporated into the A* path planning, which includes the avoidance of obstacles (blue dot line). However, the MR's plan still has many redundant points that need to be eliminated. Furthermore, the moving trajectory has not been smoothed, which also affects the turning angle of the MR when moving along the trajectory. As a result, the bird's eye view angle will also change greatly, affecting the output quality of IRDC-Net based on the monocular camera. The issue depicted in Fig. 18b persists: an excessive quantity of guiding points resulted in an escalation in the guidance trajectory of the robot, resource consumption, and processing time. To completely overcome the above problems, the improved A* algorithm was built, the results on the same map of Scenario 1 clearly show the navigation plan while ensuring all three optimal tasks: finding the shortest path, removing redundant points, and smoothing the trajectory. Furthermore, the algorithm also ensures success with safety factors included in the heuristic cost function that allows avoiding collisions with obstacles with different danger zone levels, in Fig. 18c.

In addition, the authors evaluate the performance of the GPP based on JBS-A*B algorithm continuously in Scenario 2, as shown in Fig. 19. The subsequent 50×50 grid environments are executed in a continuous fashion. The path devised by the automaton from S to G will meet all optimal requirements. In Fig. 19a, the obstacles materialized at random, and in Fig. 19b and c, the quantity of obstacles increases progressively. If only the A* path is utilized, the MR will follow the GPP based on A* with the existence of redundant

Fig. 14 The flowchart of the GPP based on JBS-A^{*}B algorithm combining with the LPP based on improved DWA



path points. A* thus necessitates a significantly greater computational footprint and memory consumption. The A* solution exhibits suboptimal performance in comparison to our enhanced A* algorithm due to processing time and path length. In addition, the A* path enters the critical region surrounding the obstacle, which is delineated by the collision cost in the grey area of Fig. 19. The utilization of path cost and collision cost in the semantic segmentation image results indicates that the MR's path exhibits enhanced performance

(indicated by red lines) within the immediate vicinity of the frontal view. Constantly beyond obstacles is a collision-free distance along the path. Finally, the path becomes smoother (green lines) as a result of the increased smooth cost components in our enhanced A*. The planning path must be longer than the trajectory.

The outcomes of a comparison between the A* algorithm and the proposed GPP based on safe JBS-A^{*}BS path planning algorithm are presented in Table 3. The comparison is

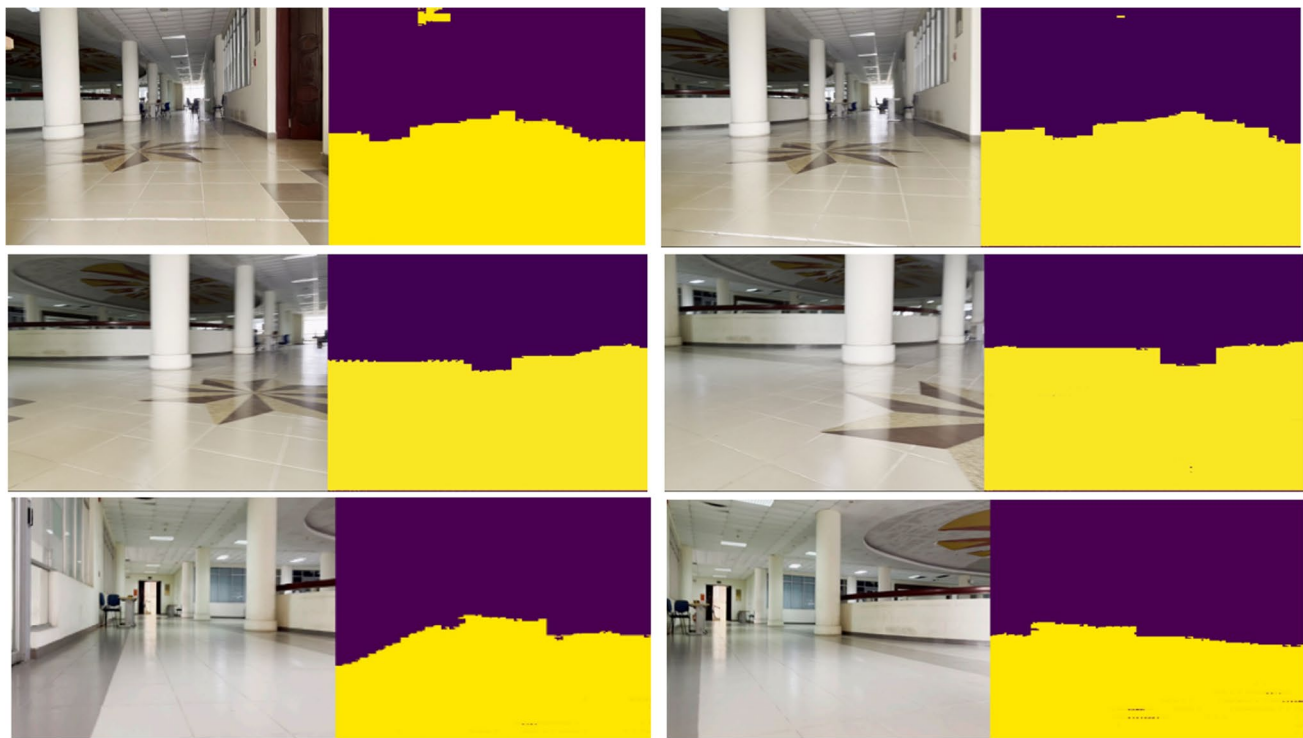


Fig. 15 Segmentation results of specific scene in TQB dataset [12] consisting of obstacles, corners, and intersection

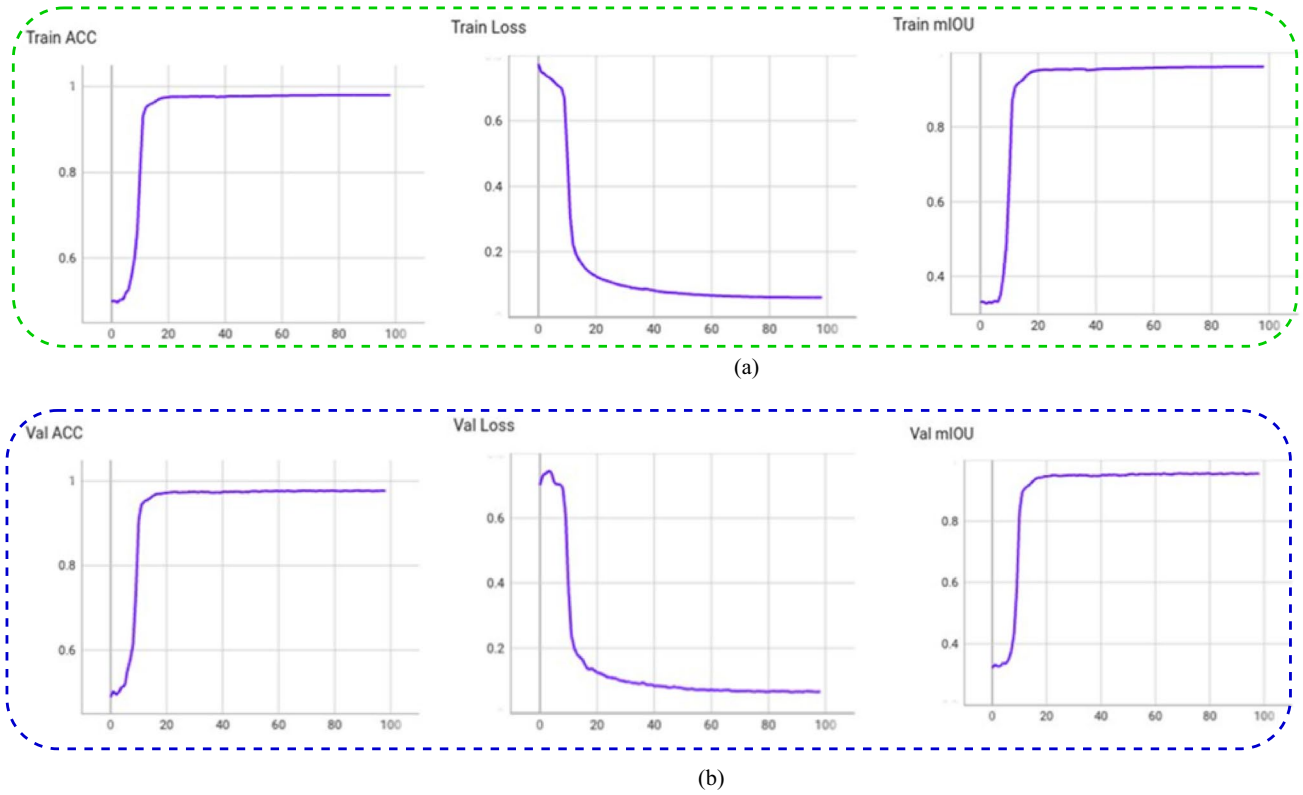


Fig. 16 Accuracy, Loss, and mIoU of IRDC-Net in (a) training and (b) validation process

Table 1 The comparison between proposed IRDC-Net with FCN-VGG 16 on the same TQB data set

Model	Accuracy	Validated mIoU	Number of training parameters
FCN-VGG 16 [4]	97.1%	71.8%	25 millions
IRDC-Net	98.3%	74.2%	3.3 millions

Table 2 The proposed segmentation model's specifications from TaQuangBuu library's data set

Train ACC	Train Loss	Train mIoU	Val ACC	Val Loss	Val mIoU
98.04	0.06	96.15	97.7	0.067	95.54

based on the path length and number of nodes traversed in the two scenarios mentioned above. A remarkable result is that the quantity of lead points is reduced and optimized. Additionally, this aids in the enhancement of path smoothing

quality and the preservation of camera stability during robot motion. Furthermore, optimal input image quality aids in the optimization of IRDC-Net's processing time and facilitates the navigation of the robot.

In Scenario 3, the MR's moving environment not only has static obstacles S_{S1} and S_{S2} , but two dynamic obstacles S_{D1} and S_{D2} will move diagonally from the top to the bottom at an angle of 45° with the speed of 0.2 m/s. Based on the global path, the MR will have to go through a narrow area Gap. The Gap will have a decreasing width because the dynamic obstacle S_{D1} moves closer to the static obstacle S_{S3} . The optimal navigation problem becomes more difficult if the MR does not establish a safe, optimal path planning in the local area based on DWA, going through the Gap, still ensuring the requirements of the global planning path is the shortest path, eliminating redundant points and smoothing MR's trajectory. Figure 20 (snapshots (a)-(f)) depicts the MR following the GPP based on safe JBS-A*B algorithm. Incorporating DWA in local areas helps the robot increase its ability to handle situations in avoiding obstacles such as Fig. 20b to d, the MR has successfully

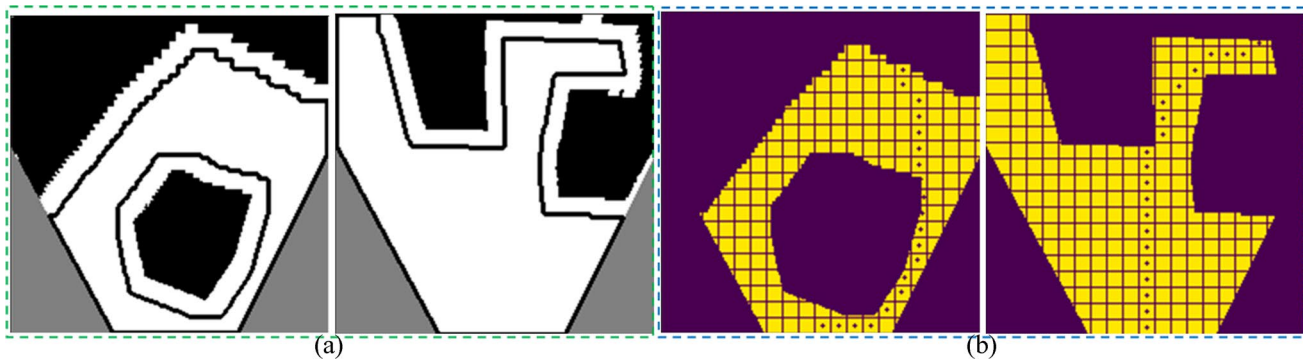


Fig. 17 MR's moving environment with (a) additional risk zones around obstacles and (b) obstacles having a risk zone in the MR's environment based on the grid-map method

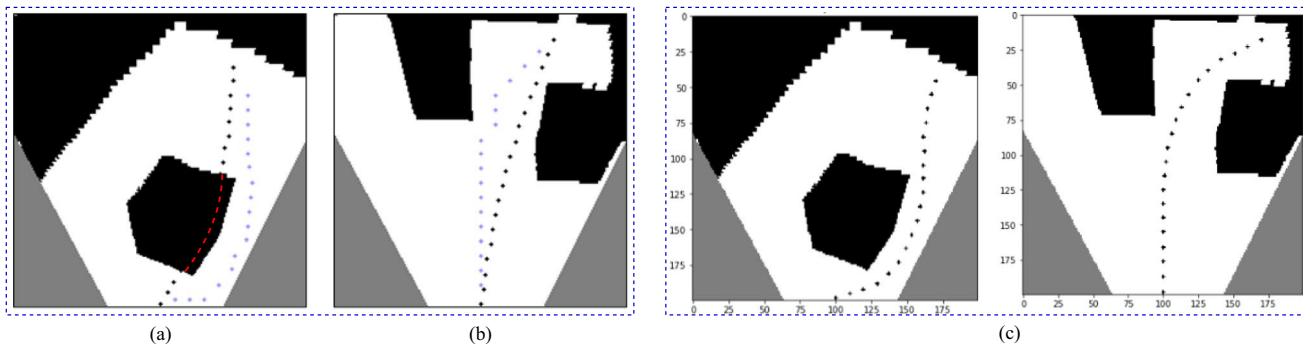


Fig. 18 The GPP based on JBS-A*B algorithm with (a): the comparison between A* algorithm without the risk zone (black line) and improved A* algorithm having the risk zone and JPS but without

smooth algorithm (blue line), (b): the comparison between A* algorithm having only the risk zone (black line) and improved A* algorithm having with the risk zone and smooth but without JPS

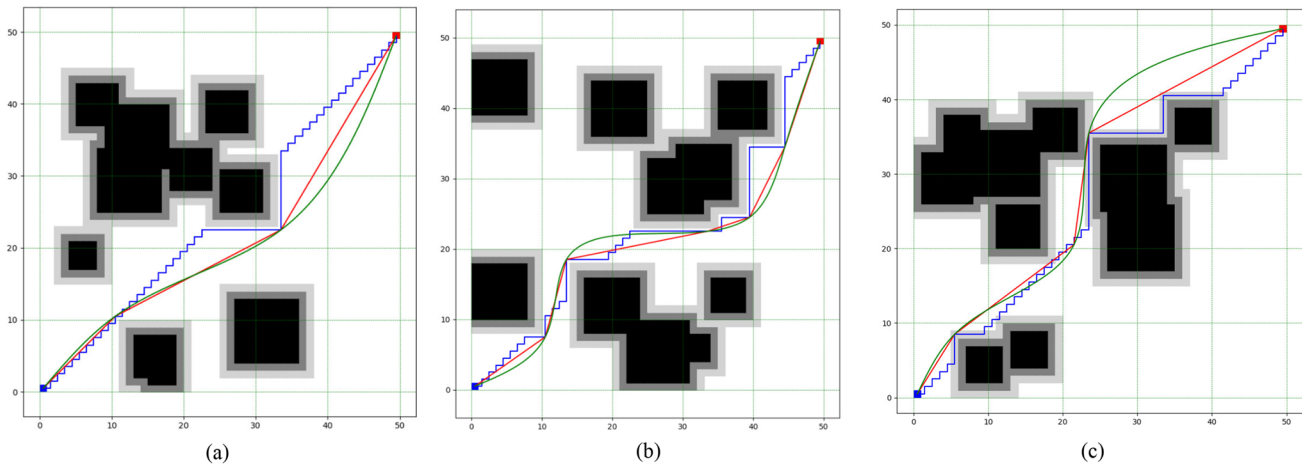


Fig. 19 The GPP based on the safe JBS-A*B algorithm in the comparison between A* algorithm (blue line), improved A* algorithm has the risk zone and JPS but without smooth algorithm (red line),

and improved A* algorithm has risk cost, JPS, and smooth algorithm (green line) in all three cases the number of obstacles gradually increases in the environment

Table 3 The comparison between the GPP based on safe JBS-A*BS path planning and different method

Methods	Figure 19a		Figure 19b		Figure 19c	
	Nodes	Length	Nodes	Length	Nodes	Length
Traditional A* algorithm [7]	77	89.8	46	86.2	58	87.3
Improved Dijkstra algorithm [6]	55	82.3	38	80.1	42	81.2
Our path planning without smooth cost [42]	4	74.3	7	70.2	5	72.6
Our path planning with all cost functions	4	74.8	7	70.6	5	72.9

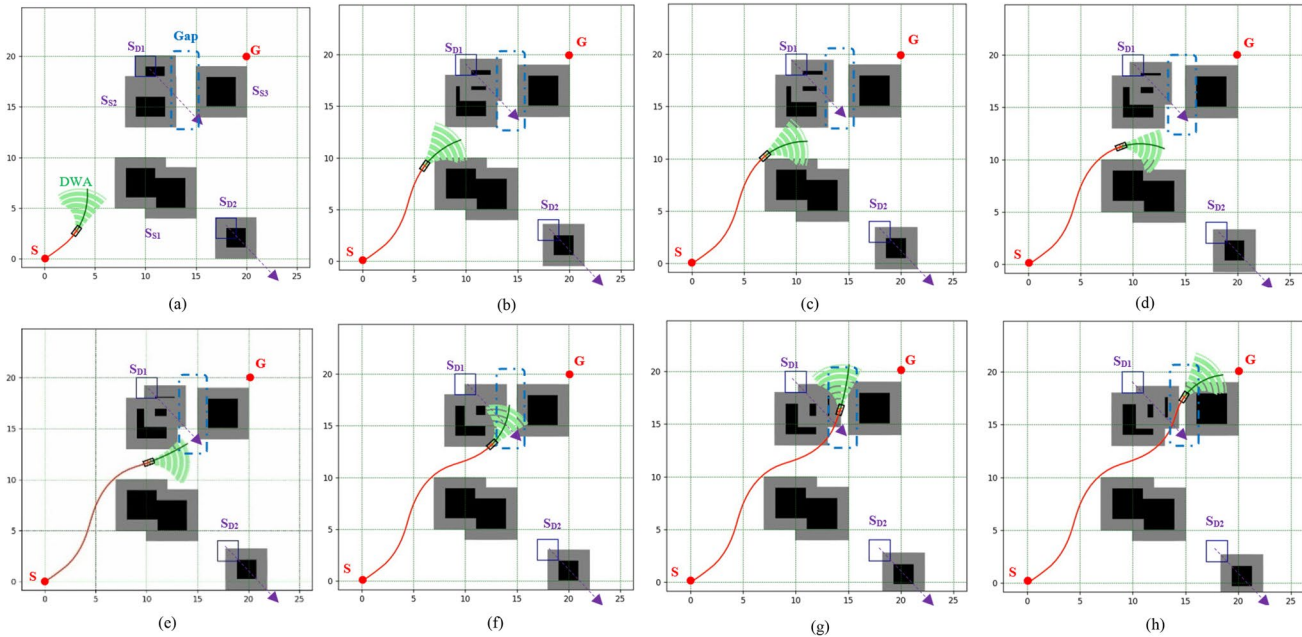


Fig. 20 The MR's path planning based on the safe JBS-A*B algorithm and DWA in the experimental moving obstacle scenario 3

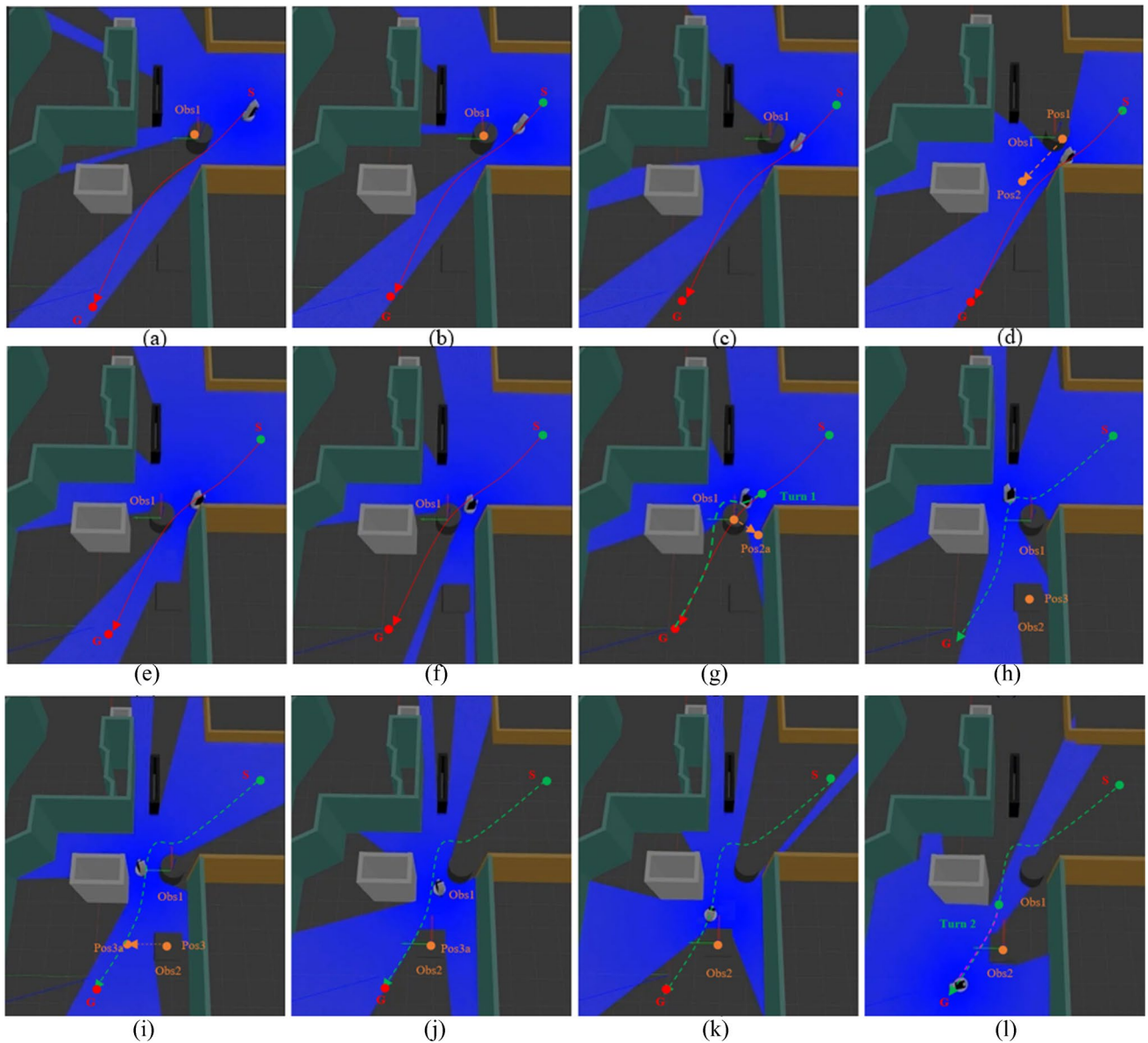


Fig. 21 The MR's path planning based on safe JBS-A*B algorithm and DWA in the experimental moving obstacle scenario in ROS environment

turned with the smallest distance to the obstacle corner S_{D1} at the first turn corner. Furthermore, when detecting a dynamic obstacle S_{D1} that tends to intersect with the global road, with improved DWA, the MR adjusts the trajectory with the appropriate speed to pass through the narrow GAP area, still ensuring to follow the predetermined GPP, successful reach to the goal point G in Fig. 20f to h.

Finally, to verify the efficacy of obstacle avoidance in a real-world intricate setting, the experiments illustrated in Fig. 21 are carried out in Scenario 4. This scenario features two dynamic obstacles, Obs1 and Obs2, that influence the original GPP. Subsequently, recalculations are made for

specific regions by adopting the DWA to modify the LPP within a Robot Operating System (ROS) framework.

The MR pursues a global path from start point S to goal point G, according to the MR navigation strategy in Fig. 14. The velocity of the obstacle Obs1 as it transitioned from position Pos 1 to Pos 2, then from Pos 2 to Pos 2a was 0.2 m/s. The obstacle Obs2 moves horizontally from position Pos3 to Pos 3a with the velocity of 0.25 m/s. Maximum velocity: 1 m/s; maximum angular velocity: 25°/s; angle velocity resolution: 1°/s; acceleration: 0.25 m/s²; and angular acceleration: 45°/s², correspondingly, were the parameters of the MR.

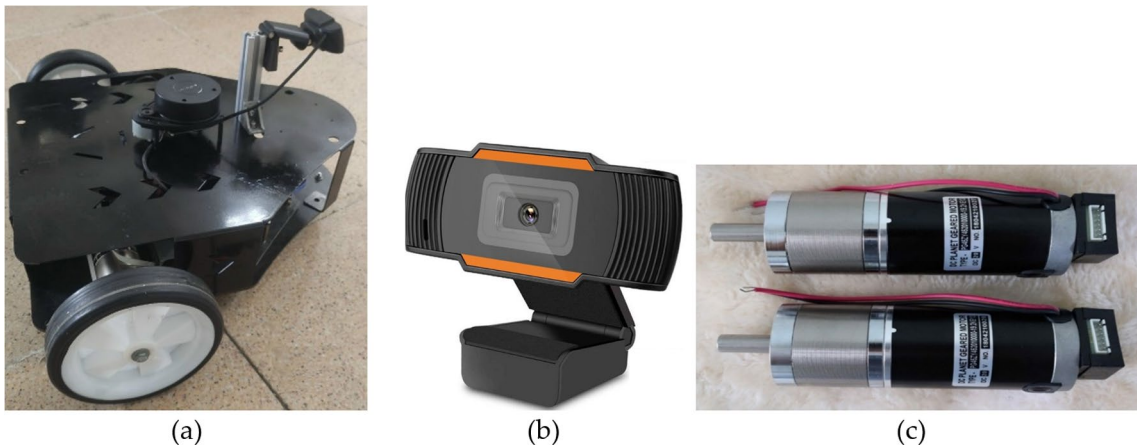


Fig. 22 The experimental three-wheeled MR: (a) MR fully equipped, (b) camera PCW01-QC with 1280×720 p resolution, and (c) servo DC 24 V—90W with the speed of 14,000 rpm and the speed after reducer of 730 rpm

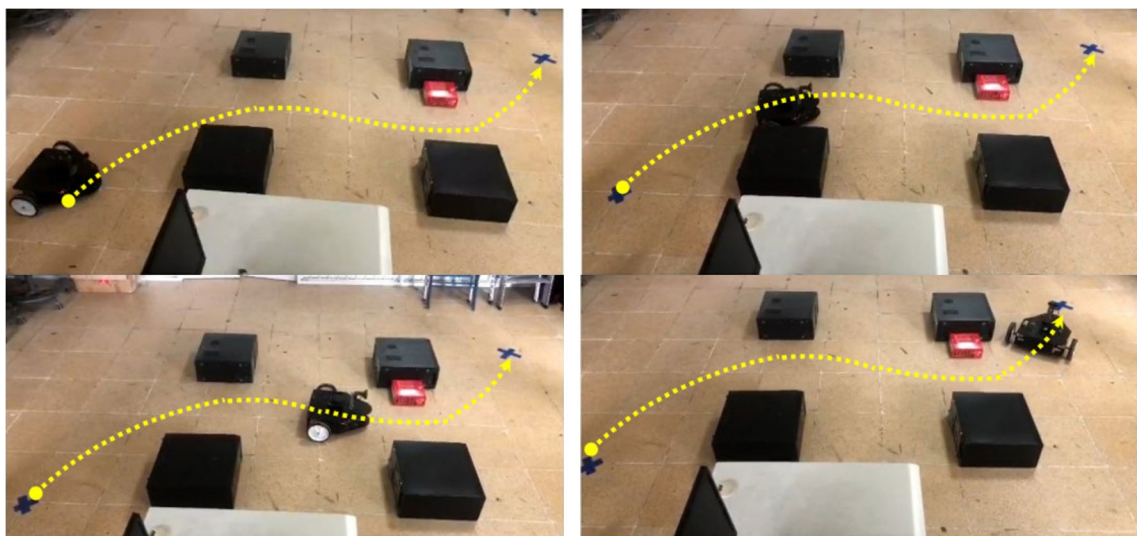


Fig. 23 MR tracks the GPP based on the safe JPS-A*B algorithm while ensuring the LPP based on improved DWA

As depicted in Fig. 21a, the MR will progress from starting point S to objective point G. The global path has been completely constructed. Within each localized region of the frontal view, the mobile robot detects the presence of obstacles along its trajectory. The mobile robot then maintains a secure distance from the obstacle Obs 1 at Pos 1, as shown in Fig. 21b, during its movement. Moreover, in accordance with safe JBS-A*BS algorithm, the path will intersect the initial global path as the Obs 1 transitions from Pos 1 to Pos 2. Failure to implement the optimized mobile robot path will result in a collision between the robot and the obstacle Obs 1 (represented by the red lines in Figures from 21e to 21 g). Based on Eq. (20), the MR's

velocity is reduced from 1 m/s to a level that allows for sufficient time to process the implementation of the optimized path. The path of the mobile robot is entirely redesigned at the turning position Turn 1, from Fig. 21g to 21j in accordance with the new path (green dashed lines). The collision situation continues to occur when obstacle Obs 2 moves horizontally, tending to intersect with the newly constructed the GPP at the upper corner of obstacle Obs 2. Because there is enough time and area and the touch is small, the robot maintains the same speed and makes small changes in the local path to form a new orange path at Turn 2, in Fig. 21l. The optimized path from S to G is effectively followed by the mobile robot, maintaining a collision-free

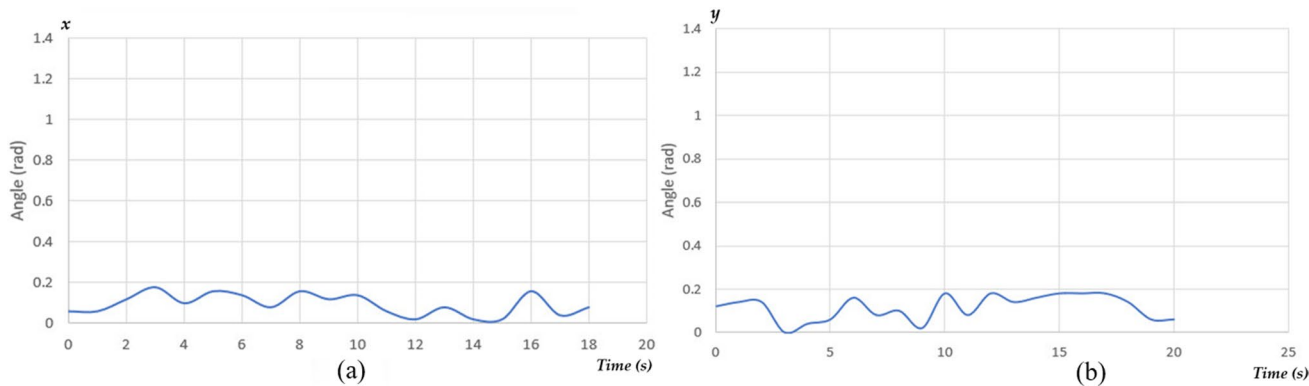


Fig. 24 Changes in steering angle while the MR tracks the trajectory **(a)** steering angle between coordinates in x axis and **(b)** steering angle between coordinates in y axis

distance of 0.2 m from the obstacle. The results of our evaluation indicate that the approach effectively identifies and circumvents obstacles in real-time with exceptional accuracy and effectiveness.

After successful testing in the ROS environment, to test the applicability in practice, the three-wheeled MR with the size of 60 cm × 50 cm, equipped with two servo DC 24 V—90W, camera PCW01-QC and Jetson nano is presented in Fig. 22. As illustrated in Fig. 23, the LPP based on improved DWA enhances the MR's ability to avoid obstacles in local regions while tracking the GPP based on the safe JPS-A*B algorithm. Based on the results obtained in [4, 12, 42], the segmentic segmentation is an essential component in the construction of the frontal perspective of the ground. Furthermore, IRDC-Net with clearly reduced training parameters combined with Adam optimization and quantization techniques help with complex indoor environmental challenges on both GPP and LPP, in real-time.

Because of the fixed camera position, the performance of the proposed semantic segmentation will be impacted by the smooth trajectory [4, 12, 39]. The GPP based on the safe JBS-A*B algorithm and improved DWA guarantees the MR tracking the trajectory with a small change of steering angle according to x and y axis. The tracking trajectory control is robust with changing the steering angle less than 0.2 radians, as shown in Fig. 24, due to the effective implementation of the MR's navigation strategy, specifically the process of refining the path while ensuring the safety of the mobile robot.

6 Conclusions

The paper addresses the complexities inherent in real-world PP mandates the resolution of multi-objective optimization challenges, encompassing the maximization of objectives such as trajectory regularity, minimum

obstacle distance, and path minimization. The utilization of data augmentation proves instrumental in predicting and navigating through challenging scenarios, including those characterized by chaotic backgrounds or low lighting conditions. Firstly, to introduce a real-time method for extracting corridor sequences from a single image. This is achieved by proposing the integration of a quantization technique with the lightweight semantic segmentation model IRDC-Net, resulting in a reduction of training parameters and computational expenses. The mean Intersection over Union (mIoU) achieves a notable value of 89%, complemented by a high accuracy rate of 98%. Subsequently, the segmentation of the ground plane and the MR's observation from an aerial perspective serve as inputs for generating a moving path, based on GPP employing the A* algorithm. However, limitations arise in GPP's inability to adapt to dynamic obstacles altering their positions. To address this, a real-time LPP mechanism based on an improved DWA is designed. Consequently, the MR's path planning, incorporating the JBS-A*B algorithm for global planning and DWA for local adjustments, adheres to an optimal navigation strategy. Subsequently, the segmentation of the ground plane and the MR's observation from an aerial perspective serve as inputs for generating a moving path, based on GPP employing the A* algorithm. However, limitations arise in GPP's inability to adapt to dynamic obstacles altering their positions. To address this, a real-time LPP mechanism based on an improved DWA is designed. Consequently, the MR's path planning, incorporating the JBS-A*B algorithm for global planning and DWA for local adjustments, adheres to an optimal navigation strategy based on IRDC-Net.

Acknowledgements This research is funded by Hanoi University of Science and Technology (HUST) under project number T2023-PC-008, Lab-506: Computer Vision and Autonomous Mobile Robot (CVMR), VJIIIST, HUST; iRobot Lab, SMAE, HaUI, Vietnam; and Mobile

Multimedia Communications Laboratory (MMC), SIT, Japan is gratefully acknowledged for providing work location, guidance, and expertise.

Author Contributions Conceptualization, T.V.D.; Methodology, T.V.D. and P.X.T.; Software, P.X.T.; Formal analysis, T.V.D. and P.X.T.; Investigation, P.X.T.; Resources, T.V.D.; Data curation, T.V.D.; Writing-original draft, T.V.D. and P.X.T.; Writing-review & editing, T.V.D. and P.X.T.; Visualization, P.X.T.; Supervision, T.V.D.; Project administration, T.V.D. and P.X.T. All authors have read and agreed to the published version of the manuscript.

Funding This research is funded by Hanoi University of Science and Technology (HUST) under project number T2023-PC-008.

Data Availability Taquangbuu library's dataset is supplied as the following link: <https://github.com/dangthaihviet/TaQuangBuu.Dataset> (accessed on 31 July 2023).

Declarations

Ethics Approval Not applicable.

Informed Consent Statement Not applicable.

Conflicts of Interest The authors declare no conflict of interest.

Institutional Review Board Statement The study was conducted in accordance with the Declaration of Helsinki and approved by the Institutional Review Board (or Ethics Committee).

Open Access This article is licensed under a Creative Commons Attribution-NonCommercial-NoDerivatives 4.0 International License, which permits any non-commercial use, sharing, distribution and reproduction in any medium or format, as long as you give appropriate credit to the original author(s) and the source, provide a link to the Creative Commons licence, and indicate if you modified the licensed material. You do not have permission under this licence to share adapted material derived from this article or parts of it. The images or other third party material in this article are included in the article's Creative Commons licence, unless indicated otherwise in a credit line to the material. If material is not included in the article's Creative Commons licence and your intended use is not permitted by statutory regulation or exceeds the permitted use, you will need to obtain permission directly from the copyright holder. To view a copy of this licence, visit <http://creativecommons.org/licenses/by-nc-nd/4.0/>.

References

- Faridi, A.Q., Sharma, S., Shukla, A., Tiwari, R., Dhar, J.: Multi-robot multi-target dynamic path planning using artificial bee colony and evolutionary programming in unknown environment. *Intel. Serv. Robot.* **11**(2), 171–186 (2018). <https://doi.org/10.1007/s11370-017-0244-7>
- Song, X., Zhijiang, Z., Liang, X., Huaidong, Z.: Monocular camera and laser based semantic mapping system with temporal-spatial data association for indoor mobile robots. *Multimed. Tools Appl.* **82**, 34459–34484 (2023). <https://doi.org/10.1007/s11042-023-14796-1>
- Maulana, I., Rasdina, A., Priamadhi, R.A.: Lidar Application for Mapping and Robot Navigation on Closed Environment. *J. Meas. Electron. Commun. Syst.* **4**(1), 767–782 (2018). <https://doi.org/10.25124/jmecs.v4i1.1696>
- Dang, T.V., Bui, N.T.: Multi-Scale Fully Convolutional Network-Based Semantic Segmentation for Mobile Robot Navigation. *Electronics* **12**(3), 533 (2023). <https://doi.org/10.3390/electronics12030533>
- Nguyen, V.T., Chu, D.T.: Study on tracking real-time target human using deep learning for high accuracy. *J. Robot.* **2023**, 9446956 (2023). <https://doi.org/10.1155/2023/9446956>
- Liu, L.S., et al.: Path planning for smart car based on Dijkstra algorithm and dynamic window approach. *Wirel. Commun. Mob. Comput.* **2021**(4), 1–12 (2021). <https://doi.org/10.1088/10.1155/2021/8881684>
- Xunyu, Z., Jun, T., Huosheng, H., Xiafu, P.: Hybrid path planning based on safe A* Algorithm and adaptive window approach for mobile robot in large-scale dynamic environment. *J. Intell. Rob. Syst.* **99**(2), 65–77 (2020). <https://doi.org/10.1007/s10846-019-01112-z>
- Lin, Z., Lu, L., Yuan, Y., Zhao, H.: A novel robotic path planning method in grid map context based on D* lite algorithm and deep learning. *J. Circuits Syst. Comput.* **33**(4), 2450057 (2023). <https://doi.org/10.1142/S0218126624500579>
- Liu, L., et al.: Global dynamic path planning fusion algorithm combining jump-A* Algorithm and dynamic window approach. *IEEE Access* **9**, 19632–19638 (2021). <https://doi.org/10.1109/ACCESS.2021.3052865>
- Yang, H., Teng, X.: Mobile robot path planning based on enhanced dynamic window approach and improved A* Algorithm. *J. Robot.* **2022**(2), 1–9 (2022). <https://doi.org/10.1155/2022/2183229>
- Zong, X., Tian, J., Hu, H., Peng, Z.: Hybrid path planning based on safe A* Algorithm and adaptive window approach for mobile robot in large-scale dynamic environment. *J. Intell. Rob. Syst.* **99**, 65–77 (2020). <https://doi.org/10.1007/s10846-019-01112-z>
- Dang, T.V., Tran, D.M.C., Tan, P.X.: IRDC-Net: lightweight semantic segmentation network based on monocular camera for mobile robot navigation. *Sensors* **23**(15), 6907 (2023). <https://doi.org/10.3390/s23156907>
- Zhao, X., Wang, Z., Huang, C., Zhao, Y.: Research on static/dynamic global path planning based on improved A algorithm for mobile. *J. Robot.* **2023**, 5098156 (2023). <https://doi.org/10.1155/2023/5098156>
- Dang, T.V., Nguyen, D.S.: Optimal navigation based on improved A* algorithm for mobile robot. *Lect. Note Netw. Syst.* **752**, 574–580 (2023). https://doi.org/10.1007/978-981-99-4725-6_68
- Zhao, X., Wang, Z., Huang, C., Zhao, Y.: Mobile robot path planning based on an improved A* algorithm. *Robot* **40**(6), 903–910 (2018)
- Tang, G., Tang, C., Claramunt, C., Hu, X., Zhou, P.: Geometric A-star algorithm: an improved A-star algorithm for AGV path planning in a port environment. *IEEE Access* **9**, 59196–59210 (2021). <https://doi.org/10.1109/ACCESS.2021.3070054>
- Song, R., Liu, Y., Bucknall, R.: Smoothed A* algorithm for practical unmanned surface vehicle path planning. *Appl. Ocean Res.* **83**(6), 9–20 (2019). <https://doi.org/10.1016/j.apor.2018.12.001>
- Zhang, H.M., Li, M.L., Yang, L.: Safe path planning of mobile robot based on improved A* algorithm in complex terrains. *Algorithms* **11**(4), 44 (2018). <https://doi.org/10.3390/a11040044>
- Tang, B., Hirota, K., Hirota, K., Wu, X., Dai, Y., Jia, Z.: Path planning based on improved hybrid A* algorithm. *J. Adv. Comput. Intell. Intell. Inform.* **25**(1), 6–72 (2021). <https://doi.org/10.20965/jaci.ii.2021.p0064>
- Wang, H., Yin, P., Zheng, W.: Mobile robot path planning based on enhanced dynamic window approach and improved A algorithm. *J. Robot.* **2022**, 2183229 (2022). <https://doi.org/10.1155/2022/2183229>

21. Wu, B., Chi, X., Zhao, C.: Dynamic path planning for forklift AGV based on smoothing A* and improved DWA hybrid algorithm. *Sensors* **22**(18), 7079 (2022). <https://doi.org/10.3390/s22187079>
22. Yasrab, R., Pound, M.P.: CNN based heuristic function for A* pathfinding algorithm: using spatial vector data to reconstruct smooth and natural looking plant roots. *bioRxiv* (2021). <https://doi.org/10.1101/2021.08.17.456626>
23. Liu, X., Zhang, D., Zhang, T.: Novel best path selection approach based on hybrid improved A* algorithm and reinforcement learning. *Appl. Intell.* **51**(9), 9015–9029 (2021). <https://doi.org/10.1007/s10489-021-02303-8>
24. Beed, R.S., Sarkar, S., Roy, A.: A Hybrid Multi-Objective Carpool Route Optimization Technique using Genetic Algorithm and A* Algorithm. *arXiv:2007.05781* (2020). <https://doi.org/10.48550/arXiv.2007.05781>
25. Tao, Y., et al.: A mobile service robot global path planning method based on ant colony optimization and fuzzy control. *Appl. Sci.* **11**(8), 3605 (2021). <https://doi.org/10.3390/app11083605>
26. Dang, T.V.: Autonomous mobile robot path planning based on enhanced A* algorithm integrating with time elastic band. *MM Sci. J.* **10**, 6717–6722 (2023). https://doi.org/10.17973/MMSJ.2023_10_2023052
27. Li, H., Zhao, T., Dian, S.: Forward search optimization and sub-goal-based hybrid path planning to shorten and smooth global path for mobile robots. *Knowl. Based Syst.* **258**(2), 110034 (2022). <https://doi.org/10.1016/j.knosys.2022.110034>
28. Hsu, C.C., Chen, Y.J., Lu, M.C., An L.S.: Hybrid path planning incorporating global and local search for Mobile robot. Conference Towards Autonomous Robotic Systems 7429 (2012). https://doi.org/10.1007/978-3-642-32527-4_50
29. Imran, M., Kunwar, F.: A Hybrid path planning technique developed by integrating global and local path planner. 2016 International Conference on Intelligent Systems Engineering (ICISE). IEEE (2016). <https://doi.org/10.1109/INTELSE.2016.7475172>
30. Wu, Q., et al.: Real-time dynamic path planning of mobile robots: a novel hybrid heuristic optimization algorithm. *Sensors* **20**(1), 188 (2019). <https://doi.org/10.3390/s20010188>
31. Kashyap, A.K., Parhi, D.R., Muni, M.K., Pandey, K.K.: A hybrid technique for path planning of humanoid robot NAO in static and dynamic terrains. *Appl. Soft Comput.* **96**, 106581 (2020). <https://doi.org/10.1016/j.asoc.2020.106581>
32. Ma, Z., et al.: A* algorithm path planning and minimum snap trajectory generation for mobile robot. 2021 4th International Conference on Robotics, Control and Automation Engineering (RCAE), 284–288 (2021). <https://doi.org/10.1109/RCAE53607.2021.9638900>
33. Kang, Y., & Victorino, A. C.: Human-vehicle cooperative driving using image-based dynamic window approach: System design and simulation. 2016 IEEE 19th International Conference on Intelligent Transportation Systems (ITSC), 2487–2492 (2016). <https://doi.org/10.1109/ITSC.2016.7795956>
34. Wang, Y., She, W., Fu, M., Ding, F., & Dai, S.: Real-time obstacle avoidance of hovercraft based on follow the gap with dynamic window approach. OCEANS 2018 MTS/IEEE Charleston, pp. 1–8 (2018). <https://doi.org/10.1109/OCEANS.2018.8604720>
35. Shelhamer, V., Long, J., Darrell, T.: Fully convolutional networks for semantic segmentation. *IEEE Trans. Pattern Anal. Mach. Intell.* **39**(4), 640–651 (2016). <https://doi.org/10.1109/TPAMI.2016.2572683>
36. Wang, C., Zhao, Z., Ren, Q., Xu, Y., Yu, Y.: Dense U-Net based on patch-based learning for retinal vessel segmentation. *Entropy* **21**(2), 168 (2019). <https://doi.org/10.3390/e21020168>
37. Yang, S., Maturana, D., & Scherer, S.: Realtime 3D scene layout from a single image using convolutional neural networks. In Proceedings of the 2016 IEEE International Conference on Robotics and Automation (ICRA), pp. 2183–2189 (2016). <https://doi.org/10.1109/ICRA.2016.7487368>
38. Qin, Y., et al.: A Rapid identification technique of moving loads based on MobileNetV2 and transfer learning. *Buildings* **13**(2), 572 (2023). <https://doi.org/10.3390/buildings13020572>
39. Dang, T.V., Bui, N.T.: Obstacle avoidance strategy for mobile robot based on monocular camera. *Electronics* **12**(8), 1932 (2023). <https://doi.org/10.3390/electronics12081932>
40. Mei, R., Wang, Z., & Chen, X.: CRNN-ResNet: Combined CRNN and ResNet Networks for OFDM Receivers. *IEEE Transactions on Cognitive Communications and Networking (Early Access)*. (2024). <https://doi.org/10.1109/TCCN.2024.3378225>
41. Liu, M., Yao, D., Liu, Z., Guo, J., Chen, J.: An improved adam optimization algorithm combining adaptive coefficients and composite gradients based on randomized block coordinate descent. *Comput. Intell. Neurosci.* **2023**(5), 1–14 (2023). <https://doi.org/10.1155/2023/4765891>
42. Kostková, J., Flusser, J., Lébl, M., Pedone, M.: Handling Gaussian Blur without Deconvolution. *Pattern. Recognit.* **103**(2), 107264 (2020). <https://doi.org/10.1016/j.patcog.2020.107264>
43. Aghajarian, M., McInroy, J.E., Muknahallipatna, S.: Deep learning algorithm for Gaussian noise removal from images. *J. Electron. Imaging* **29**(4), 1 (2020). <https://doi.org/10.1117/1.JEI.29.4.043005>
44. Tsubota, K., Aizawa, K.: Comprehensive comparisons of uniform quantization in deep image compression. *IEEE Access* **11**(1), 4455–4465 (2023). <https://doi.org/10.1109/ACCESS.2023.3236086>
45. Hartley, R., Kissnerman, A.: Multiple View Geometry in Computer Vision. Cambridge University Press, Cambridge, UK (2000)

Publisher's Note Springer Nature remains neutral with regard to jurisdictional claims in published maps and institutional affiliations.

Thai-Viet Dang Assoc. Pro. Dr. Thai-Viet Dang holds a PhD of Electrical Engineering, College of Electrical Engineering and Computer Science, NCU, Taiwan (2012). He also received his Engineer of Automation (2001) and Master of Automatic Control (2007), HUST. He is currently a senior lecturer in Mechatronics Dept., SME, HUST. He achieved the title of Associate Professor of Mechatronic (2023). He is a member of Council of Asian Science Editor (CASE). His research is such as: Autonomous Mobile Robot, Computer Vision, IoT Systems and Controller-based Observer design and STEM/STEAM Education based on deep technology.

Phan Xuan Tan Received the B.E. degree in Electrical-Electronic Engineering from Military Technical Academy, Vietnam, M.E. degree in Computer and Communication Engineering from Hanoi University of Science and Technology, Vietnam and Ph.D. degree in Functional Control Systems from Shibaura Institute of Technology, Japan. He is currently an Associate Professor at Shibaura Institute of Technology. His current research interests include Deep learning for Visual Computing, Image and Video Processing, Computational Light field, 3D View Synthesis, Multimedia Quality of Experience, Multimedia Networking.